

Univerzita Karlova

Přírodovědecká fakulta

Studijní program: B-GEOL



Grigorii Shmelev

Marinní sedimenty typu red beds z pánve Adana (východní část Středoziemního moře) – zkoumání podmínek jejich vzniku a jejich paleoenvironmentální význam

The Adana basin marine red beds (Eastern Mediterranean Sea) – investigating their origin and paleoenvironmental significance

Bakalářská práce

Vedoucí práce/Školitel: RNDr. Filip Scheiner, Ph.D.

Praha, 2024

Charles University

Faculty of Science

Study programme: B-GEOL



Grigorii Shmelev

The Adana basin marine red beds (Eastern Mediterranean Sea) – investigating their origin and paleoenvironmental significance

Marinní sedimenty typu red beds z pánve Adana (východní část Středoziemního moře) – zkoumání podmínek jejich vzniku a jejich paleoenvironmentální význam

Bachelor's thesis

Supervisor: RNDr. Filip Scheiner, Ph.D.

Prague, 2024

Declaration

I declare that this thesis has been composed solely by myself and that it and that I have listed all sources and literature used. Neither this thesis nor any substantial part of it has been submitted for another or the same academic degree.

Prague, 30.7 2024

Grigorii Shmelev

Prohlášení

Prohlašuji, že jsem závěrečnou práci zpracoval samostatně a že jsem uvedl všechny použité informační zdroje a literaturu. Tato práce ani její podstatná část nebyla předložena k získání jiného nebo stejného akademického titulu.

V Praze, 30.7 2024

Grigorii Shmelev

Acknowledgments

I would like to thank my supervisor RNDr. Filip Scheiner, Ph.D. for his enormous patience and help with my bachelor's thesis in every minute I needed and from every corner of the world. I would also like to thank prof. RNDr. Katarína Holcová, CSc. for finding new possibilities for me to learn more about the subject of my thesis. Also, I would like to thank prof. Dr. Atike Nazik from the Çukurova Üniversitesi in Adana, southern Turkey for professional advices.

Abstract

The aim of this bachelor thesis is to compile basic characteristics of the so-called marine red beds (MRBs; <15 wt.% Fe), in particular their formation processes and paleoenvironmental significance, as well as their distribution in the sedimentary record. Furthermore, the practical part of this thesis focuses on Miocene marine sequences from the Adana Basin, Turkey, Eastern Mediterranean Sea. Using foraminifera as paleobiological markers, three samples from reddish colored marine deposits, stratigraphically ranging from the Burdigalian to the Serravallian, were analyzed to reconstruct the paleoenvironmental conditions. The interpretations are based on the presence of various foraminiferal ecological markers in the studied assemblages along with different statistical indices (e.g., Enhanced Benthic Foraminiferal Oxygen Index, Simpson and Shannon diversity indices). The results suggest an oligotrophic, warm water, open ocean environment with periods of water column instability, and a highly oxic benthic environment from the outer shelf to the bathyal zone (CAR 9 sample).

Abstrakt

Cílem této bakalářské práce je kompilace základních charakteristik tzv. pestrých vrstev mořského původu (charakteristických svým červeným zbarvením; MRB; <15 hm. % Fe), a to zejména procesů jejich vzniku, jejich paleoenvironmentální význam, a to včetně jejich výskytu v globálním sedimentárním záznamu. Dále se praktická část této práce zaměřuje na analýzu miocenních marinních sedimentů typu MRB z pánve Adana v Turecku, z východního Středomoří. Práce analyzuje tři vzorky z různých stratigrafických úrovní (Burdigalu až Serravalu) za účelem rekonstrukce paleoenvironmentálních podmínek pomocí analýzy společenstev foraminifer. Interpretace jsou založeny na přítomnosti různých ekologických markerů, foraminifer, ve studovaných společenstvech spolu s různými statistickými indexy (např. Enhanced Benthic Foraminiferal Oxygen Index, Simpsonův a Shannonův index diversity). Výsledky naznačují oligotrofní prostředí otevřeného moře s periodami eutrofizace vodního sloupce, a dále s vysoce oxickým bentickým prostředím vnějšího šelfu po bathyální zónu (vzorek CAR 9).

Table of Contents

1. Introduction	1
2. Marine red beds	1
2.1. Definition	1
2.2. General characteristics of MRBs	1
2.3. Proterozoic MRBs	2
2.4. Phanerozoic MRBs	3
2.4.1. Cambrian MRBs	4
2.4.2. Devonian MRBs	4
2.4.3. Triassic MRBs	5
2.4.4. Jurassic MRBs	5
2.4.5. Cretaceous MRBs	6
2.5. Cenozoic MRBs	7
3. A case study from the Miocene sequences of the Adana Basin, Turkey, Eastern Mediterranean	7
3.1. Time frame and geological setting	7
3.1.1. Miocene	7
3.1.2. Adana Basin, Turkey	9
3.2. Foraminifera as paleoindicators	12
3.3. Materials and methods	13
3.4. Results	15
3.5. Discussion	20
4. Conclusions	22
5. References	23
6. WWW resources	35

1. Introduction

The aim of this thesis is to provide an overview of marine red beds sedimentary deposits, including their characteristic features, global distribution throughout geological history and the various hypotheses explaining the origin of the characteristic/distinctive red pigmentation in these deposits. In addition, this thesis briefly illustrates the application of paleontological methods, particularly paleobiological analysis based on foraminiferal assemblages, to reconstruct the paleoenvironmental settings of three selected samples belonging to marine red beds deposits from the Adana Basin, Turkey.

2. Marine red beds

2.1. Definition

In general, red beds facies or deposits (characterised by <15 wt% Fe) are common in sedimentary successions, but most formed in terrestrial settings (hence termed continental red beds) where the main colouring agent (most commonly hematite) was developed under oxygenated atmospheric conditions (e.g., Turner, 1980). In contrast, marine red beds (abbreviated MRBs), otherwise also known as oceanic red beds (ORBs), are reddish to pinkish to brownish coloured sediments deposited in marine environments that have been coloured due to changes in seawater chemistry in response to fluctuations of climatic and oceanographic factors during their deposition and subsequent diagenesis (Kiipli et al., 2000). It is worth noting that these deposits should not be confused with iron formations (IFs; ≥ 15 wt % Fe), which were deposited mainly from the Neoproterozoic to the Paleoproterozoic (~2.8–1.8 Ga) and at ~ 0.8 Ga in the Neoproterozoic (e.g., Bekker et al., 2010; Konhauser et al., 2017)

2.2. General characteristics of MRBs

MRBs have been reported from a wide range of depositional settings, from shallow marine, to continental slopes and rises, to oceanic ridges and deep basins below the CCD (carbonate compensation depth; Wang *et al.*, 2011; Hu *et al.*, 2005). In terms of lithology, these reddish coloured beds mainly include hemipelagic and pelagic limestones and marly limestones, marlstones and marly shales, calcareous shales, and less commonly radiolarian cherts that occur below the CCD (Luan *et al.*, 2019; Widiatama *et al.*, 2021). Different hypotheses explain the origin of red pigmentation of limestones and shales: i) iron of detrital origin that was derived from continental weathering (Franke & Paul, 1980), ii) iron-bacterial mediation during MRB sedimentation (Mamet & Pr eat, 2006), and iii) iron oxidation in an oligotrophic and highly oxic environment (Lyu *et al.*, 2022).

The red coloration is usually attributed to the presence of crystalline ferric (Fe³⁺) oxides, goethite (FeO(OH)) and hematite (Fe₂O₃; Elorza *et al.*, 2021; Giosan *et al.*, 2002). However, the red colouration decreases as either the degree of crystallinity or the grain size of the hematite mineral increases (Zhang *et al.*, 2014; He *et al.*, 2023). In addition, Mn²⁺-bearing calcite contributes to the red colouration (Card & Montenari, 2023), while iron-bearing minerals, such as chlorite and illite give the layers a greenish colour (Zhang *et al.*, 2014). Furthermore, the different red, pink and greenish-yellow colours of these deposits reflect a sedimentation rate and/or oxidation capacity of the water mass from which they originate (Table 1; Elorza *et al.*, 2021). This is helpful in terms of paleotemperature reconstructions as shown by e.g. Brett *et al.* 2012, who associates reddish lithologies with periods of relatively cooler conditions, mirroring the greenhouse-icehouse transitions.

Table 1. Presumed paleoenvironmental conditions (temperature and oxidation capacity) of water masses at the seafloor explaining particular colouring in the marl-limestone couplets (modified from Elorza *et al.*, 2021).

No.	Water mass Conditions	Marl-limestone couplet
1.	Water mass with high oxidation capacity and sufficient thickness	Pink marls and limestones, red marls and limestones
2.	Water mass with sufficient oxidation capacity, but without achieving material oxidation	Purple marls and limestones
3.	Water mass with limited oxidation capacity, without achieving complete oxidation	Purple marls, yellowish-grey limestones
4.	Rapid change in the oxidation capacity of the water mass towards more oxidising and cold waters	Modification from grey couplets to greenish-yellow to red couplets
5.	No oxidation capacity of the water mass	Grey marls and limestones

2.3. Proterozoic MRBs

The first prominent MRBs (<15 wt% Fe) occurred discontinuously during the Paleo- to Meso-Proterozoic era and they are known from deposits in Northern Canada (~1.9 Ga; Hodgskiss & Sperling, 2019) and Northern China (~1.5–1.4 Ga; Wang *et al.*, 2017; Tang *et al.*, 2020; Zou *et al.*, 2020). The mid-

Proterozoic era is generally characterised by a low-productivity biosphere (e.g., Anbar & Knoll, 2002; Reinhard *et al.*, 2017; Crockford *et al.*, 2018; Hodgskiss *et al.*, 2019). Therefore, the formation of MRBs during this period was most likely due to purely geochemical processes. There are some studies that have investigated the environment and formation mechanism of Paleo- to Meso-Proterozoic MRBs. These studies, including those by Tang *et al.* (2020), Wang *et al.* (2017), and Zou *et al.* (2020), present several different views on their origin.

i) Tang *et al.* (2020) observed that these red beds do not differ in Fe(II) content, but have elevated Fe(III) content compared to the adjacent non-beds. This study suggests that the studied Xiamaling MRBs were formed by intrusion of anoxic, Fe²⁺-rich deep waters into moderately oxygenated shallow waters.

ii) On the other hand, the study by Zou *et al.* (2020) suggests that the formation of the MRBs in the Yangzhuang Formation (~1.5 Ga) required subaerial exposure in a supratidal environment during marine regression, mainly for the Fe²⁺ oxidation.

iii) In addition, Wang *et al.* (2017) proposed two complementary models for the origin of these studied MRBs. The first model is consistent with the findings of Zou *et al.* (2020) emphasising an enhanced vertical mixing of shallow oxygenated waters with deeper layers of Fe²⁺-rich waters. The second model considered the study by Lenton & Daines (2017). It was suggested that the iron concentration of subsurface water masses was much higher during the Meso-Proterozoic than that during the Phanerozoic (~1 µM vs >4 nM). Therefore, it is proposed that the occurrence of mid-Proterozoic MRBs represents a rise in atmospheric oxygen levels, reaching over 4% of the current atmospheric levels, at about 1.4 Ga (Chen *et al.*, 2022).

A summary by Wang *et al.* (2022) concluded that Meso-Proterozoic MRBs were deposited in a redox-stratified ocean, where anoxic deep waters (rich in hydrothermal Fe²⁺) were overlain by more oxygenated surface waters. Additionally, there are well-documented Neo-Proterozoic marine red beds, mainly from the Cryogenian (720–635 Ma) and Ediacaran (635–539 Ma) periods. Cryogenian MRBs are commonly developed as oolitic carbonates in shallow-water settings (e.g., Chen *et al.*, 2022). Furthermore, Bai *et al.* (2020) analysed geochemical indicators during the Marinoan Ice Age (654–632 Ma) in the Nantuo Formation and suggested that periods of warmer paleoclimate caused partial melting of glaciers, which had a positive impact on the supply of oxidised iron to the marine environments, preceding the formation of the MRBs (Ziegler & McKerrow, 1975).

2.4. Phanerozoic MRBs

The broadest range of MRBs is found in the Phanerozoic Eon, including five documented Phanerozoic MRB intervals that are spread globally: Cambrian, Late Devonian, Early Triassic, Jurassic and, undoubtedly, Cretaceous period (e.g., Franke & Paul, 1980; Li *et al.*, 2019; Michalzik, 1991; Miki,

1992). The key feature that distinguishes the Phanerozoic MRBs depositional environments from Proterozoic ones is the presence of aerobic bacteria that oxidise Fe^{2+} near the sediment surface, contributing to the reddening of the upper layers of the sediments (Mamet & Pr eat, 2006).

2.4.1. Cambrian MRBs

The first globally widespread Phanerozoic MRBs occurred during the Cambrian period. The Stage 3 of this period provided the most favourable conditions for the global formation of MRBs (Li *et al.*, 2023). Numerous studies have documented the existence of these distinctive red sedimentary deposits in various regions of the globe, including Mongolia, Russia, Australia, USA, Spain, Ireland, and many parts of China (e.g., Cordie *et al.*, 2019a; Kouchinsky *et al.*, 2022; Alexander *et al.*, 2001; Cordie *et al.*, 2019b; Rushton *et al.*, 2011). Jiang *et al.* (2009) suggested that the Cambrian MRBs correlate with periods of oceanic anoxia and also with periods of euxinia, which were periods of highly stratified waters with no oxygen and elevated levels of hydrogen sulphide (H_2S ; Gill *et al.*, 2011). By studying the Stage 3 MRBs from the Hannan-Micangshan area of southern China, Li *et al.* (2023) concluded that red beds were common in two different types of environments: i) in oxygenated littoral zones, where there was dissolved iron availability and diagenetic alteration of iron hydroxides; and ii) in deeper suboxic neritic environments with much slower sedimentation rates due to fine-grained turbidity clouds, that favoured the absorption of hematite and goethite.

2.4.2. Devonian MRBs

One of the best examples of Devonian MRBs can be found in the Prague Basin in the Czech Republic. By analysing spectral reflectance data, B abek *et al.* (2021) reported that the submicronic iron oxide in the studied MRBs is hematite - the main red colouring agent, while white and grey facies lack the hematite peak but exhibit distinct goethite peaks. Submicronic hematite has also been found within endoskeleton plates of echinoderms, providing a strong evidence for the authigenic origin of hematite. Other studies, including those made by Franke & Paul (1980) and Yuan *et al.* (2012), suggested that in situ mineralization of hematite is strong evidence for an oxygenated marine environment. Furthermore, B abek, *et al.* (2021) proposed that the primary colouring agent of MRBs (hematite) was formed by the activity of iron-oxidising bacteria during the precipitation of detrital Fe-phyllsilicates, Fe-bearing aluminosilicates and goethite dehydration. An earlier study of B abek *et al.* (2018) also revealed that during the period of the sedimentation of these Devonian MRBs, atmospheric CO_2 concentrations, mean air temperature at the Earth's surface and silicate weathering rates decreased, while atmospheric oxygen levels increased significantly.

2.4.3. Triassic MRBs

During the Early Triassic period, MRBs emerged following the Permian-Triassic boundary Oceanic Anoxic Events (OAE), as documented by Wignall & Twitchett (1996). One of the examples can be found in the Nanpanjiang Basin in the South China, where MRBs are predominantly observed in continental slope environments, with only sporadic occurrences in shallow-water carbonate platforms (Chen *et al.*, 2015).

2.4.4. Jurassic MRBs

The best known MRB facies of the Jurassic period are the so-called Ammonitico Rosso. These are widely distributed in the Tethys area, such as in Spain, Italy, Switzerland, Austria, Czech Republic, Poland, former Yugoslavia, Hungary, Bulgaria, Romania, Morocco, Algeria, Greece and Turkey. Two main studies have investigated the depositional environment and formation mechanisms of Jurassic MRBs.

i) The study by Song *et al.* (2017) suggests that the primary driving factor behind the formation of global Jurassic MRBs are OAEs (oceanic anoxic events). In particular, the Triassic–Jurassic boundary OAE (Van De Schootbrugge *et al.*, 2013) and the Toarcian OAE (Jenkyns, 1988). According to their findings, OAEs led to elevated dissolved ferrous iron (Fe^{2+}) concentrations ($>4 \text{ nM Fe}$), which is a strong precursor for the formation of MRBs.

ii) In contrary, Mamet & Pr at (2006) found that red pigmentation in the Ammonitico Rosso facies is not directly linked to elevated dissolved (Fe^{2+}) iron concentrations. Surprisingly, they reported that samples from the red facies showed no significant difference in the iron content (350 ppm) compared to the adjacent grey facies. They further emphasise that the mineralogical expression of iron played a crucial role in determining the colour of these facies. Therefore, Mamet & Pr at (2006) proposed an alternative explanation. According to their hypothesis the red colour results from the dispersion of submicrometric hematite in the case of the red facies, while in the case of the grey facies iron ions remain trapped in the calcite lattice. Their model further suggests that submicrometric hematite forms near the sediment interface due to the activity of Fe^{2+} oxidising bacteria. Additional insights come from studies by Gillan & De Ridder (2018) on modern sediments. This study highlighted the significance of steep dysoxic–anoxic gradients at a millimetre to centimetre scales. When these interfaces or settings are available, they are rapidly colonised by iron-oxidising bacteria.

2.4.5. Cretaceous oceanic red beds or CORBs

The Cretaceous period is notable for being one of the most thoroughly studied intervals in case of marine red beds. Known as CORBs or Cretaceous oceanic red beds, they occur e.g., in the Tethyan deposits in the Carpathians (e.g., Melinte-Dobrinescu *et al.*, 2009, Skupien *et al.*, 2009), in the Southern and Austrian Alps (Wagreich & Krenmayr, 2005), in the western Himalayas (Li *et al.*, 2011), in the Northern Caucasus (Cumberpatch *et al.*, 2021) and in England (Bailey, 2020).

CORBs have been reported to occur first locally during the Berriasian–Barremian stages (145–121 Ma; Neumann & Wagreich, 2009) and then globally in the Aptian–Albian stages (121–100 Ma) of the Lower Cretaceous (Xi *et al.*, 2007) and in the Early Turonian (Wendler & Kuss, 2009). Nevertheless, the most extensive red bed time interval is the late Cretaceous, mainly, the Campanian–Maastrichtian stages (84–66 Ma). It is worth noting that most of the late-Cretaceous red deposits extend into the Palaeocene (Ahmed *et al.*, 2017). While most of the Phanerozoic MRBs are predominantly of deeper marine origin, the Cretaceous ORBs occur in a range of bathymetric conditions from shallow platform sections to offshore slope to pelagic basin. For instance, red shales in the Tethyan Himalaya of the southern China were deposited in shallow marine environments, whereas red facies deposition in the same stage in the northern China were limited to continental slope environments (e.g., Li *et al.*, 2009, Li *et al.*, 2011). Using chronostratigraphic data, Hu *et al.* (2012) distinguished two groups of CORBs based on their durations: short-term CORBs and long-term CORBs.

i) Short-term CORBs are commonly less than 1 Ma in their respective stratigraphic duration. They are deposited in deeper marine environments, where the influence of terrigenous runoff into a basin is assumed to be minimal (e.g., Hu *et al.*, 2012). Thus, other factors come into effect, namely, the Milankovitch cycles. These cycles are generally associated with positive fluctuations in carbon production and decrease in argillaceous content within the deposit during the first half of the cycles. During the latter half, carbon production decreases, whilst the second parameter raises. According to Bailey (2020) the increased content of argillaceous minerals is thought to have a strong positive link to the red beds deposition.

ii) The second group, long-term CORBs, are much longer in their respective stratigraphic durations (persisting for more than 4 Ma). Several studies attribute the deposition of long-term CORBs to an abrupt change in ocean oxygenation as a consequence of the OAEs (e.g., C. Wang *et al.*, 2011; Wagreich *et al.*, 2011). The increased burial of organic carbon and pyrite associated with the OAEs probably led to a substantial reduction in atmospheric CO₂ concentrations, which is thought to have caused a significant global climate cooling during and after the OAEs. As a result, the formation of cold deep ocean waters increased, enhancing their oxidising capacity due to an increase in dissolved oxygen content and thus, promoting the formation of oceanic red beds.

The other two main accepted conditions that favour the development of CORBs include low sedimentation rates and low concentrations of organic nutrients in seawater (Neuhuber *et al.*, 2007). When oligotrophic conditions coincide with low sedimentation rates, this implies that only a limited amount of organic matter can precipitate, thus reducing the likelihood of formation of redox conditions and maximising the probability of ferric iron formation (Hu *et al.*, 2012).

2.5. Cenozoic MRBs

In general, MRBs in the Cenozoic Era are not as prominent as in the Phanerozoic. There are no globally widespread deposits that can be associated with MRBs, but there are a number of isolated deposits or facies in different regions that can be considered as MRBs. These are often associated with specific environmental conditions that led to their formation. To illustrate, this study further analyses Miocene sequences from the Adana Basin, Turkey, Eastern Mediterranean, which are known for their reddish colour and they are associated with marine origin (Nazik, 2004).

3. A case study from the Cenozoic – Miocene sequences of the Adana Basin, Turkey, Eastern Mediterranean

As part of my bachelor's thesis, I analysed three samples from the Miocene deposits of the Adana Basin, Turkey, which is located in the Eastern Mediterranean area, using foraminiferal markers, and palaeobiological indices based on the composition of foraminiferal assemblages.

3.1. Time frame and geological setting

3.1.1. Miocene

The Miocene epoch spans from 23 to 5.33 Ma and is divided into 6 stages. Listed in order from oldest to youngest: Aquitanian, Burdigalian, Langhian, Serravallian, Tortonian and Messinian (Table 2).

In terms of global climate, during the Miocene the Earth was generally in an icehouse state, one of the two main climatic states of the Earth, characterised by the existence of large ice sheets at both poles (Thomas, 2008). However, during the Middle Miocene, the climate rapidly switched to a warm “greenhouse” setting (a state with a severe reduction of polar ice sheets; Gasson *et al.*, 2016), known as the Miocene Climate Optimum (MMCO or MCO) with a greatly reduced East Antarctic Ice Sheet (EAIS; e.g., Gasson *et al.*, 2016; Zachos *et al.*, 2001). For example, during the MCO, the global mean annual temperature (MAT) was about ~18.4°C, which is about 1.4°C higher than reported for the Early Miocene (Steinthorsdottir *et al.*, 2021; You *et al.*, 2009; Super *et al.*, 2018). The MCO was followed by the Middle Miocene Climate Transition (MMCT, ~15–13.7 Ma; e.g., Mourik *et al.*, 2011; Flower & Kennett, 1995),

characterised by global cooling during the upper Langhian to the Serravallian stages, which shifted the Earth back to an “icehouse” setting (Zachos et al., 2008). One of the key events was the expansion of the Antarctic ice sheet, which marked the beginning of the second period of the Miocene icehouse climate (Zachos et al., 2001; Westerhold et al., 2020). For example, during the Middle Miocene Climatic Transition (MMCT) in Eskihisar, northern Turkey, the MAT decreased to ~15.2–18 °C (Bouchal et al., 2018; Tzanova et al., 2015).

Table 2. Neogene stratigraphic table (modified from <https://stratigraphy.org>).

Period	Epoch	Stage	Numerical age (Ma)	Analysed samples
N E O G E N E	Pliocene	Piacenzian	3.6 – 2.6	X
		Zanclean	5.3 – 3.6	X
	<u>(studied epoch)</u> Miocene	Messinian	7.2 – 5.3	X
		Tortonian	11.6 – 7.2	X
		Serravallian	13.8 – 11.6	CAR 9
		Langhian	16 – 13.8	CAR B2, CAR 10
		Burdigalian	20.4 – 16	
		Aquitanian	23 – 20.4	X

The Miocene represents a crucial period regarding the evolution of the Mediterranean marine realm. During this period, many global and regional factors, such as geodynamic evolution, the closure of the Indian-Mediterranean gateway and associated palaeoceanographic overturns, affected the paleoceanography of the Mediterranean, which in turn affected carbonate production (Gueguen et al., 1998; Roca et al., 1999; Bialik et al., 2019; Rogerson et al., 2012). This triggered, for example, the biocalcification crisis and the Early Miocene Carbon Maximum (EMCM) in the central Mediterranean carbonate platforms during the Aquitanian (23–20.4 Ma), when facies dominated by LBF (Larger Benthic Foraminifera) assemblages were replaced by facies dominated by planktonic foraminifera assemblages (Brandano et al., 2015). From the late Burdigalian, the onset of the closure of the Indian-Mediterranean gateway resulted in

a progressively restricted connection with the Indian Ocean, causing the transition of the entire region to a semi-enclosed setting, associated with major paleoceanographic overturns in terms of circulation and water mass distribution (Meijer et al., 2004; Abrantes et al., 2010; Cornacchia et al., 2018). This, together with intense geodynamic activity marked by local volcanism, led to the demise of the LBF assemblages and the onset of carbonate ramps dominated by red algae and bryozoans during the middle Miocene to the Tortonian (Cornacchia et al., 2021).

3.1.2. Adana Basin, Turkey

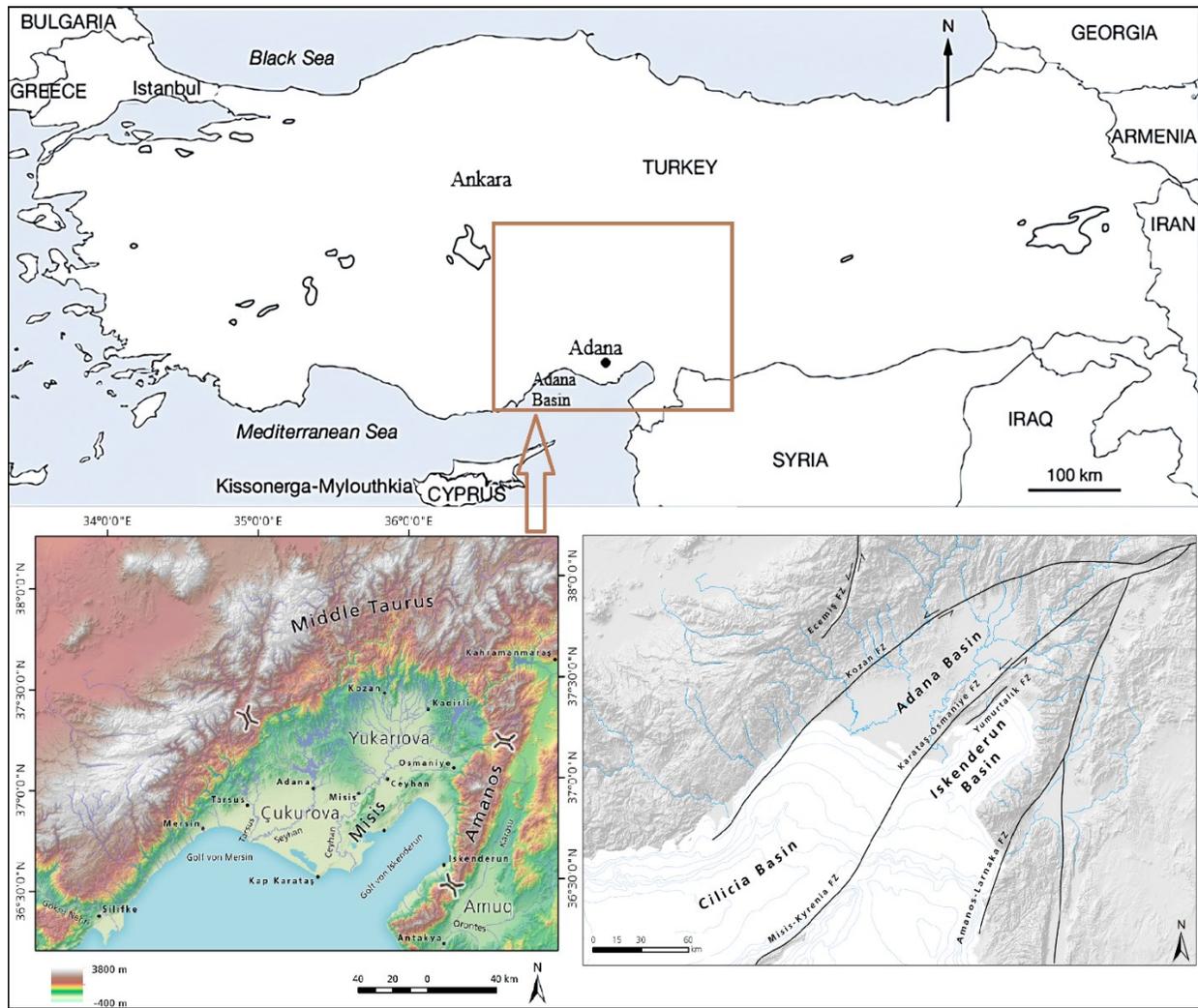


Figure 1. Map of the Adana Basin (modified from Gündem, 2019 and Rutishauser et al., 2017).

The tectonic evolution of the Anatolian micro-plate (south-eastern Turkey) has been largely controlled by a strike-slip deformation accompanied by extensional and compressional components during the Neogene (Kelling *et al.*, 1987; Karig & Kozlu, 1990). The study area - the Adana Basin (Figure 1) is one of three parts of the Anatolian micro-plate that lie directly to the southwest of the Maras triple junction (Anatolian, African and Arabian plates). The Adana Basin covers an area of approximately 10 000 km² (Burton, 2002), and is bounded by the Taurus Mountains in the north and west, by the Misis Mountains in the east, by the Mediterranean Sea in the south and in the southwest it merges with the marine Inner Cilicia Basin (Burton-Ferguson *et al.*, 2005). The Adana basin is thought to have formed as an effect of intra-plate extension in response to the initiation and evolution of the Maras triple junction (Aksu *et al.*, 1992). Exploratory drilling in the Adana Basin has revealed a Miocene to Recent succession with maximum thicknesses exceeding 4–6 km, unconformably overlying a deformed, partially eroded pre-Miocene basement (Burton-Ferguson *et al.*, 2005). The terrestrial exposure of the Adana Basin has allowed surface sampling and mapping of the basement and overlying successions. Yetiş *et al.* (1995) divide the Miocene sedimentary succession in the Adana Basin into three groups of sedimentary deposits: i) pre-transgressive deposits, ii) transgressive deposits and iii) regressive deposits, which are further divided into seven lithostratigraphic formations based on a number of unique spatial, temporal and lithologic attributes. Listed from oldest to youngest the Gildirli, Kaplankaya, Karaisali, Cingöz, Güvenç, Kuzgun and Handere formations form the Miocene to Pliocene succession of the Adana Basin (Figure 2). The Gildirli Formation, which occurs only in the north, is the oldest Neogene rock unit in the Adana Basin and was formed prior to the regionally extensive Early Miocene marine transgression (Derman & Gürbüz, 2007). The general lithological characteristics of the Gildirli Formation indicate deposition in a predominantly terrestrial environment (Williams *et al.*, 1995). The middle succession within the Adana Basin consists of lower to middle Miocene transgressive siliciclastic deposits, including the Kaplankaya, Karaisali, Cingöz and Güvenç formations (Yetiş *et al.*, 1995). The shallow marine Kaplankaya Formation was interpreted to have formed during the first transgression in the Early Miocene. The reefal benthic foraminiferal-algal and globigerinid-algal packstone (limestone) of the Karaisali Formation was formed during the upper Burdigalian (Görür, 1979; Görür, 1994). The Cingöz formation has been interpreted as a thick submarine turbidite fan complex (Silva *et al.*, 2020). Its age was determined to be Langhian–Serravallian based on foraminifera contents (Nazıklmaz & Gürbüzlmaz; 1992). The Cingöz Formation is followed by a thick succession of Burdigalian–lower Tortonian basinal shales of the Güvenç Formation, which represent a continental slope to deep marine environment. During the Middle to Late Miocene transition, the Adana Basin recorded a regressive event with the deposition of lower Tortonian fluvio-deltaic terrestrial red beds of the Kuzgun Formation (Faranda *et al.*, 2013). The Late Miocene shallow marine lagoonal-continental

deposits of the Handere Formation, succeed the Kuzgun Formation (Nazik, 2004). Evaporites of the Handere Formation are sterile and their thickness is ~3.5 m (Darbaş & Nazik, 2010).

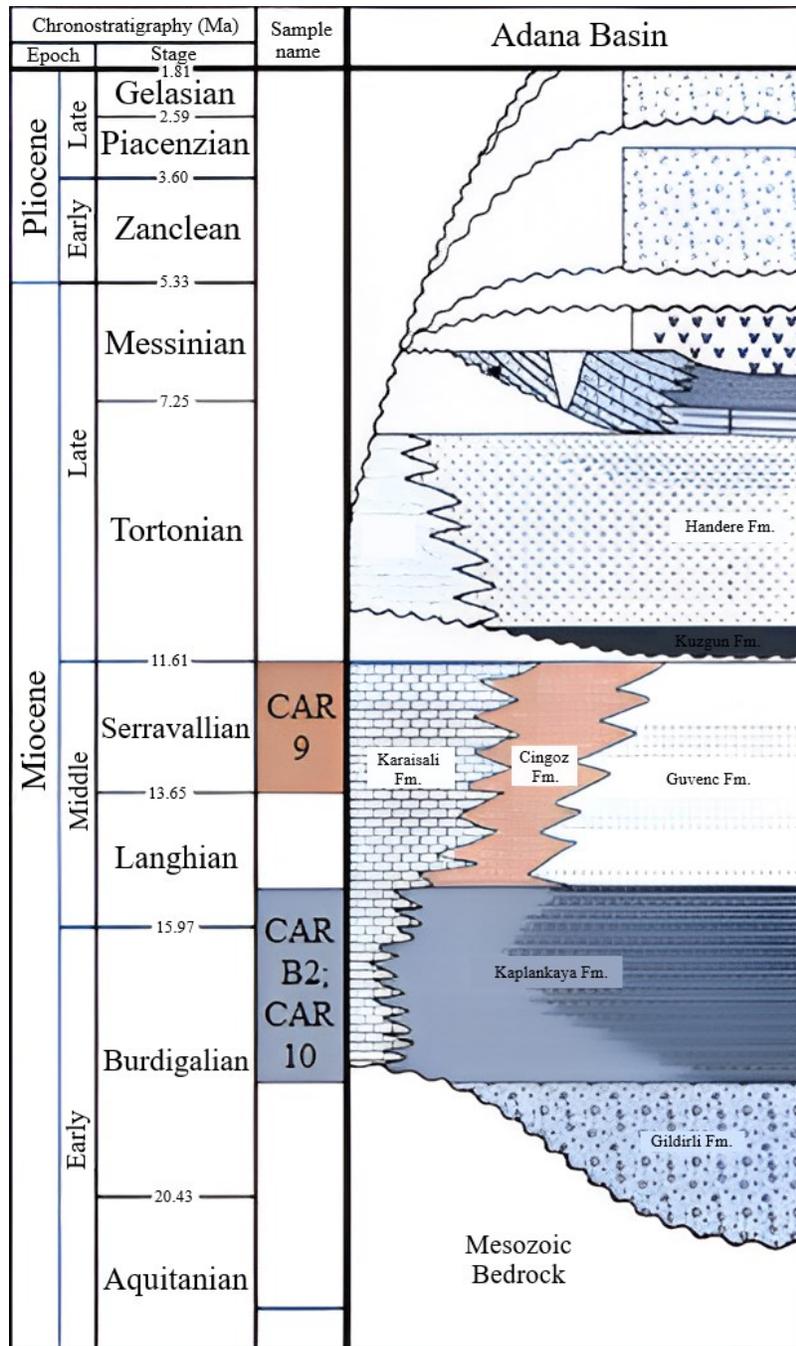


Figure 2. A simplified stratigraphic scheme of the Adana Basin (modified from Ilgar et al., 2013).

Regarding the biostratigraphy, the planktonic foraminiferal biozones identified within the Neogene sequence of the Adana Basin are: *Globigerinoides (Trilobatus) trilobus* and *Praeorbulina glomerosa curva* (Burdigalian), *Orbulina suturalis* (Langhian), and *Globorotalia mayeri* (Serravallian). The Late Tortonian is characterised by the first occurrence of *Globorotalia suterae*. There are no planktonic foraminiferal zones in the Messinian. The Pliocene is represented by the *Sphaeroidinellopsis* Acme Zone (Nazik, 2004).

The practical part of this thesis focuses on 3 samples of marine origin characterised by reddish colour and containing abundant foraminifera: i) CAR B2 falls stratigraphically into the *Trilobatus trilobus* biozone, which corresponds to the shallow marine Kaplankaya formation of the Adana Basin. It consists of interbedded sandstones and siltstones, fossiliferous marls and sandy limestones of the Burdigalian to the lower Langhian age (Yetiş, 1988); ii) CAR 9 stratigraphically falls within the *Globorotalia mayeri* biozone, which corresponds to the Serravallian age of the Cingöz formation. It consists of different flysch facies composed of conglomerates and thick-bedded sandstones (Uchman & Demircan, 1999); iii) finally, sample CAR 10 that stratigraphically falls into the *Praeorbulina glomerosa curva* and the *Trilobatus trilobus* biozone. It corresponds to the same formation as the CAR B2 – the Kaplankaya formation.

3.2. Foraminifera as palaeoindicators

As such, MRB deposits often comprise a group of facies where saline or brackish waters intrude into various marginal environments and extensive oxidation tends to remove much of the skeletal biotic record. One of the primary groups of organisms that can help to reconstruct these types of palaeoenvironments and can also be used for biochronostratigraphy and paleobiology even in marine/continental transition zones are foraminifera (e.g., Saraswat, 2015).

Foraminifera are widespread unicellular protist organisms, which are commonly used in paleontological reconstructions. They make their shells called “tests”, from various types of materials, including calcite, agglutinated sediment particles, aragonite, silica or chitin (Boltovskoy & Wright, 2013). There are also groups of foraminifera that do not produce or create any test, but these have no paleontological significance since none of their parts can be fossilised under standard conditions (Bernhard *et al.*, 2013; Pawlowski *et al.*, 2003). Overall, foraminiferal abundance, rapid diversification, relatively small biological niches and excellent preservation in the sedimentological record make them one of the most important fossil organisms used for biostratigraphy and paleoecology (Serra-Kiel *et al.*, 1998; King *et al.*, 2020). For example, foraminiferal morphology, growth and distribution are strongly affected by temperature, food and light availability in the environment (Figure 3; Fairbanks *et al.*, 1982; Caron *et al.*, 1987; Bijma *et al.*, 1990). Moreover, planktonic foraminiferal tests (from suborder Globigerinina; Figure 3) are one the most commonly used paleoceanographic proxies by terms of morphology of their tests (e.g.,

the *Globorotalia truncatulinoides* stratification index is used for reconstruction of upper ocean stratification and fluctuations in the depth of the permanent thermocline; Steph *et al.*, 2009; Feldmeijer *et al.*, 2015) or as a substrate for extraction of various geochemical signals (Kučera, 2007). In addition, the chemical composition of foraminiferal calcite is an important proxy that allows reconstructions of past seawater chemistry, biogeochemical cycles, temperature, salinity, ice volume, circulation patterns and paleoproductivity and many others (e.g., Henderson, 2002). A specific example could include: i) reconstruction of the vertical structure of the ocean by using the difference in a geochemical proxy for temperature ($\delta^{18}\text{O}$ or Mg/Ca, Sr/Ca) between near-surface and deep-dwelling species (e.g., Cléroux *et al.*, 2008; Evans *et al.*, 2016; Sagawa *et al.*, 2012); or ii) $\delta^{11}\text{B}$, which serves as a robust proxy for seawater *pH* (e.g., Ni *et al.*, 2007; Foster & Rae, 2016) and hence assessing past changes in CO_2 concentrations (e.g., Hönisch and Hemming, 2005).

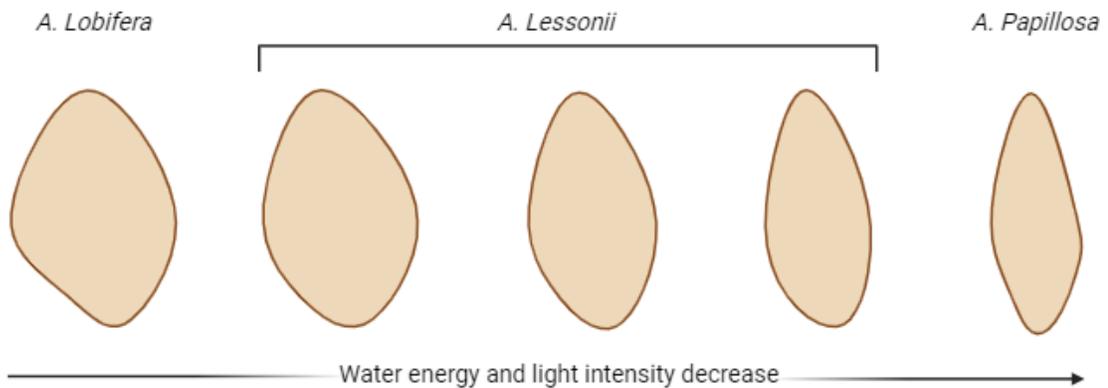


Figure 3. Silhouettes illustrating the range of shapes in three Indo-Pacific species of *Amphistegina*: (1) *A. lobifera*, high-energy, high-light environment; (2) *A. lessonii*, moderate-energy, high-light environment; (3) *A. lessonii*, low-energy, moderate-light environment; (4) *A. lessonii*, low-energy, low-light environment; and (5) *A. papillosa*, low-energy, very low light environment (Created with BioRender.com; modified from Hallock & Glenn, 1986).

3.3. Materials and methods

This study analyses three samples – CAR B2, CAR 9 and CAR 10, which come from the reddish coloured marine deposits with the abundant presence of foraminifera (see chapter 3.1.2.).

The selected samples were repeatedly washed with tap water and wet sieved to a fraction of 0.063–2.0 mm. After washing, the samples were dried at a low temperature. To quantify foraminiferal abundance,

approximately 110–160 foraminifera were handpicked from a fraction of 0.063–2.0 mm under binocular microscope. They were further examined under the scanning electron microscope (SEM; JEOL JSM-6380LV housed at the Institute of Geology and Paleontology, CUNI; Figure 4) to assess their preservation state and to observe small morphologic structures to allow precise taxonomic determination. The taxonomic identification of the foraminifera was done according to the following taxonomic references: <https://www.microtax.org>, <https://marinespecies.org> and foraminiferal plates made by prof. Atike Nazik (personal communication).

Furthermore, based on the quantitative foraminiferal data this study applies several selected statistical methods. The Enhanced Benthic Foraminifera Oxygen Index (EBFOI; Kranner et al., 2022) is an improved version of the BFOI index (Kaiho, 1994), which has been widely used to reconstruct the amount of dissolved oxygen (DO) on the seafloor and to detect changes in biodiversity. Unlike the original BFOI index, which uses only calcareous foraminifera, EBFOI uses all types of benthic foraminifera tests and divides them into dysoxic (D in the formulas), suboxic (S) and oxic (O) indicators. The detailed classification of the foraminiferal species as the indicators can be found in the supplementary materials in Kranner *et al.* (2022). Depending on the abundance of the indicators (D vs S vs O), the EBFOI can be calculated using three different formulas: i) formula 1 is used when oxic indicators are abundant; ii) if oxic indicators are few or they are absent, formula 2 is used; iii) finally, if both, oxic and dysoxic indicators are abundant in the sample, but oxic indicators are less abundant than dysoxic indicators, formula 3 is used. Finally, formula 4 is used to calculate the dissolved oxygen (DO) based on the EBFOI index. EBFOI and the DO were calculated for the sample CAR 9 using the benthic foraminiferal assemblage data. Metrics that were calculated using the PAST software (Natural History Museum of Oslo; Hammer *et al.*, 2001) to identify paleoenvironmental-bound patterns within the planktonic foraminifera assemblages in all analyzed samples are: i) species richness (total number of species identified), ii) relative abundance of different taxa and genera (percentage, showing species representation in an assemblage), iii) the Shapiro-Wilk test for normal distribution (the *p*-value greater than 0.05 shows that the data are normally distributed; González-Estrada & Cosmes, 2019), iv) the Simpson diversity index (varies from 0 to 1; account both the number of species present and the relative abundance of each species; diversity increases as species richness and evenness increase; Fallaw, 1979) and v) the Shannon index (entropy index, which varies from 0 for communities with only one taxon to high values for communities with many taxa, each with few individuals; Hammer *et al.*, 2001).

$$(1) EBFOI = 100 \left(\frac{O}{(O+D+\frac{S}{2})} \right)$$

$$(2) EBFOI = 50 \left(\frac{S}{(S+D)} - 1 \right) + O$$

$$(3) EBFOI = \frac{100 \left(\frac{O}{(O+D+\frac{S}{2})} \right) + 50 \left(\frac{S}{(S+D)} - 1 + \frac{O}{2} \right)}{2}$$

$$(4) DO \left[\frac{ml}{l} \right] = 5.28475 * e^{0.00616 * EBFOI} - 3.78475$$

3.4. Results

The results are presented for the individual samples sorted based on their age from the Middle Burdigalian to the Serravallian.

i) In sample CAR B2, 161 foraminifera specimens were identified (Table 3; Figure 5). No benthic foraminifera were present, the assemblage consisted only of planktonic foraminifera. The most abundant planktonic foraminifera species are *Trilobatus trilobus* (33 specimens), *Trilobatus quadrilobatus* (27 specimens) and *Globigerinoides ruber* (20 specimens). The *p*-value of the Shapiro-Wilk test for normal distribution is 0.00025 (Figure 8). The Simpson Index is 0.896 and the Shannon index is 2.57.

Table 3. The species representation in the sample CAR B2.

CAR B2					
Species	<i>Trilobatus trilobus</i>	<i>Trilobatus Quadrilobatus</i>	<i>Trilobatus Immaturus</i>	<i>Trilobatus sacculifer</i>	<i>Globigerina bulloides</i>
Quantity	33	27	5	3	8
Species	<i>Globigerina Falconensis</i>	<i>Globigerinoides bulloideus</i>	<i>Globigerinoides ruber</i>	<i>Globigerinoides sp.</i>	<i>Dentoglobigerina altispira</i>
Quantity	1	4	20	1	7
Species	<i>Dentoglobigerina globosa</i>	<i>Dentoglobigerina venezuelana</i>	<i>Globoquadrina dehiscens</i>	<i>Orbulina universa</i>	<i>Praeorbulina glomerosa</i>
Quantity	1	8	14	1	3
Species	<i>Praeorbulina curva</i>	<i>Praeorbulina transitoria</i>	<i>Globorotalia hirsuta</i>	<i>Globorotalia sp.</i>	<i>Globigerinella obesa</i>
Quantity	7	3	1	4	10

ii) In sample CAR 9, 116 foraminifera specimens were identified in the assemblage, of which 95 specimens are planktonic and 21 are benthic (Table 4; Figure 6). The most abundant planktonic foraminifera species

are *Globorotalia* sp. (14 specimens), *Turborotalita* sp. (13 specimens), *Fohsella* sp. (10 specimens) and *Trilobatus trilobus* (10 specimens). The most abundant benthic foraminifera species are *Heterolepa dutemplei* (12 specimens) and *Martinotiella communis* (5 specimens). The *p*-value of the Shapiro-Wilk test for normal distribution is 0.081 (Figure 8). The Simpson index is 0.932 and the Shannon index is 2.792.

Table 4. The species representation in the sample CAR 9.

CAR 9					
Species	<i>Turborotalita</i> sp.	<i>Fohsella</i> sp.	<i>Globorotalia mayeri</i>	<i>Orbulina bilobata/universa</i>	<i>Praeorbulina curva</i>
Quantity	13	10	5	6	4
Species	<i>Globorotalia</i> sp.	<i>Globorotalia suterae</i>	<i>Dentoglobigerina Venezuelana/altispira</i>	<i>Globigerinoides ruber</i>	<i>Globigerina bulloides</i>
Quantity	14	5	8	9	1
Species	<i>Globoquadrina dehiscens</i>	<i>Trilobatus trilobus</i>	<i>Trilobatus sacculifer</i>	<i>Trilobatus quadrilobatus</i>	<i>Neogloboquadrina humerosa</i>
Quantity	5	10	1	2	2
Species	<i>Uvigerina</i> sp.	<i>Martinotiella communis</i>	<i>Bolivina</i> sp.	<i>Heterolepa</i> sp.	
Quantity	2	5	2	12	

iii) In sample CAR 10, 107 foraminifera specimens were identified in the assemblage, of which 101 specimens were planktonic and 6 benthic (Table 5; Figure 7). The most abundant planktonic foraminifera species are *Trilobatus trilobus* (27 specimens), *Globoquadrina dehiscens* (20 specimens) and *Praeorbulina glomerosa* (20 specimens). The most abundant benthic foraminifera species is *Uvigerina* sp. (4 specimens). The *p*-value of the Shapiro-Wilk test for normal distribution is 0.0005659 (Figure 8). The Simpson index is 0.863 and the Shannon index is 2.3.

Table 5. The species representation in the sample CAR 10.

CAR 10					
Species	<i>Praeorbulina glomerosa</i>	<i>Praeorbulina curva</i>	<i>Praeorbulina transitoria</i>	<i>Trilobatus trilobus</i>	<i>Trilobatus quadrilobatus</i>
Quantity	18	5	1	27	4
Species	<i>Globoquadrina dehiscens</i>	<i>Dentoglobigerina venezuelana/altispira</i>	<i>Orbulina suturalis</i>	<i>Globorotalia</i> sp.	<i>Globigerina bulloides</i>
Quantity	20	3	4	2	9
Species	<i>Globigerinoides ruber</i>	<i>Globigerinoides sacculifer</i>	<i>Fohsella</i> sp.	<i>Uvigerina</i> sp.	<i>Heterolepa dutemplei</i>
Quantity	5	2	1	4	2

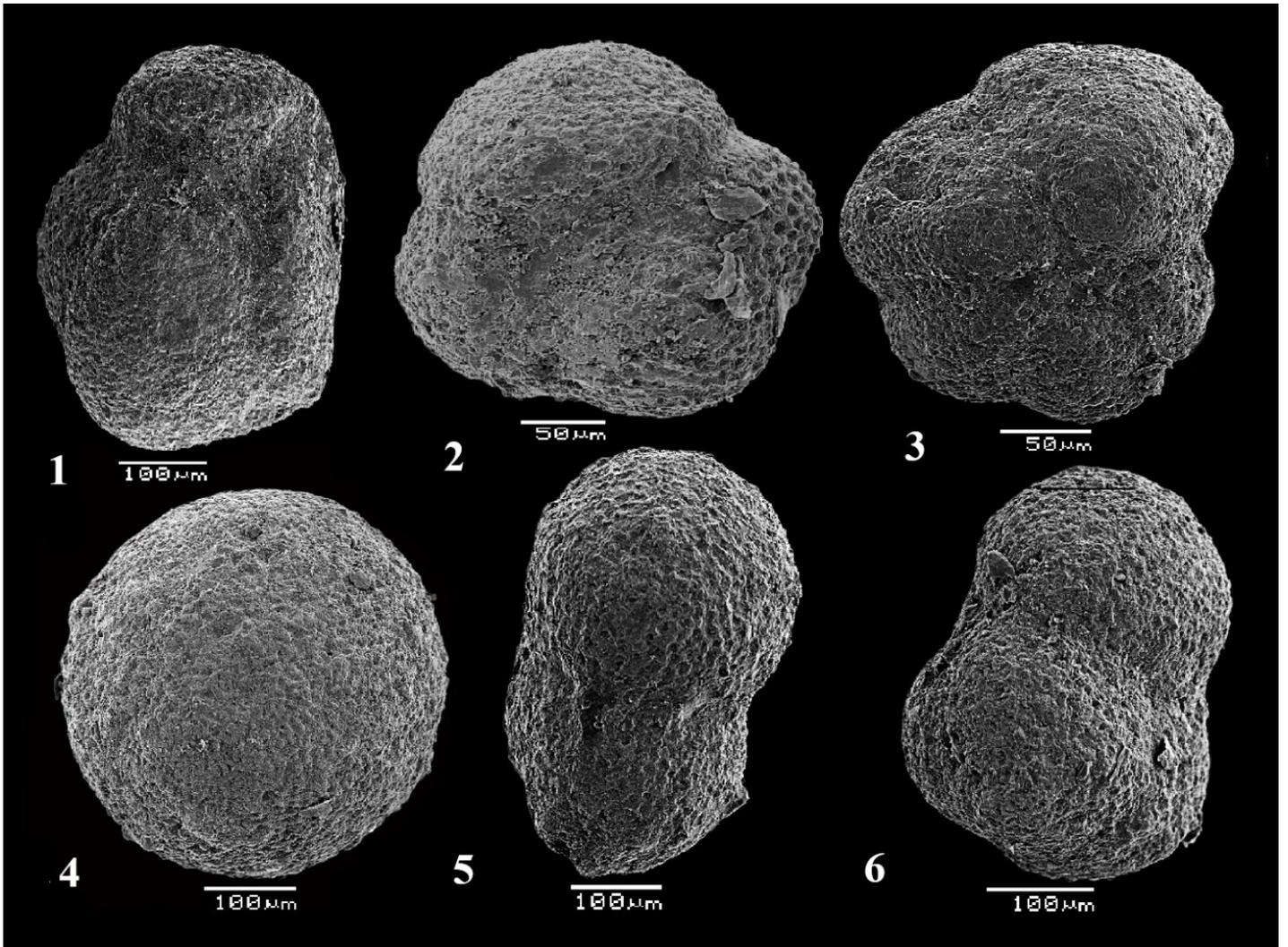


Figure 4. Selected foraminifera identified in the analysed samples from the Adana Basin (SEM images): (1) *Globigerina venezuelana* (Hedberg); (2) *Globigerina falconensis* (Blow) (3) *Globorotalia (Globoconella) praescitula* (Bandy); (4) *Orbulina suturalis* (Brönnimann); (5) *Praeorbulina transitoria* (Blow) (6) *Trilobatus trilobus* (Reuss).

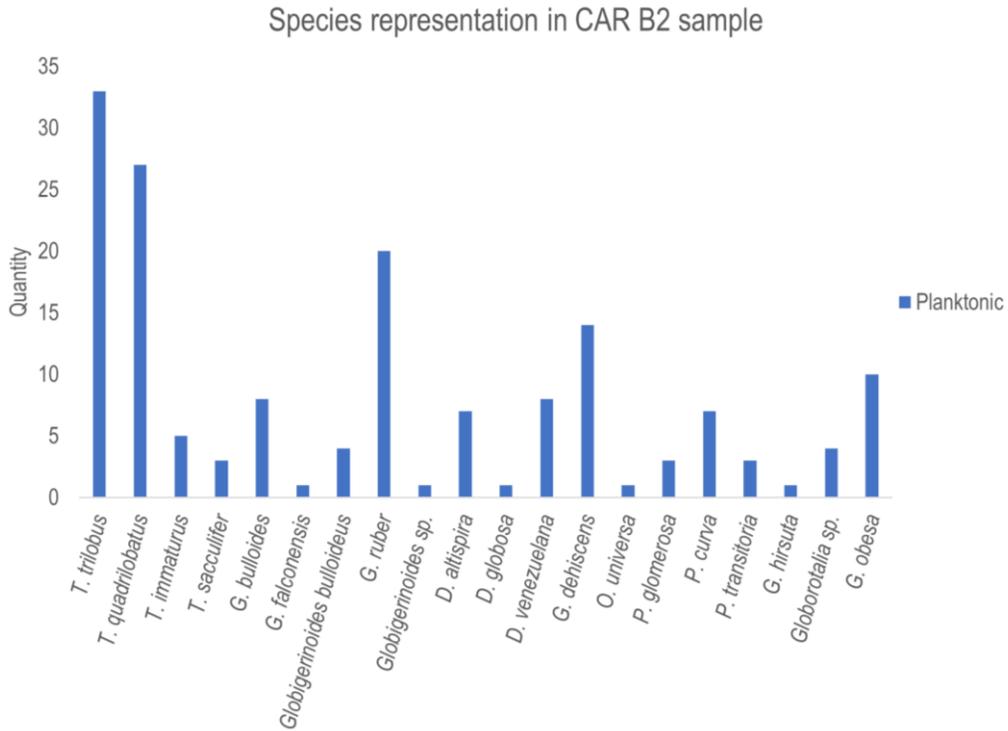


Figure 5. Identified foraminiferal species and their abundance in the CAR B2 sample.

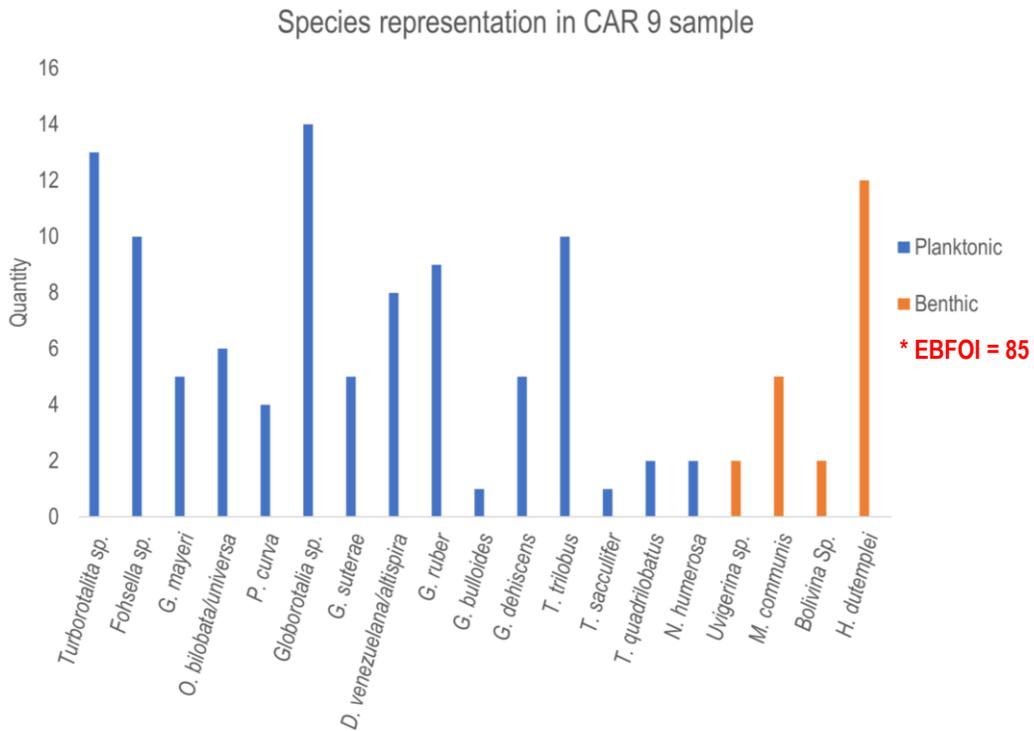


Figure 6. Identified foraminiferal species and their abundance in the CAR 9 sample.

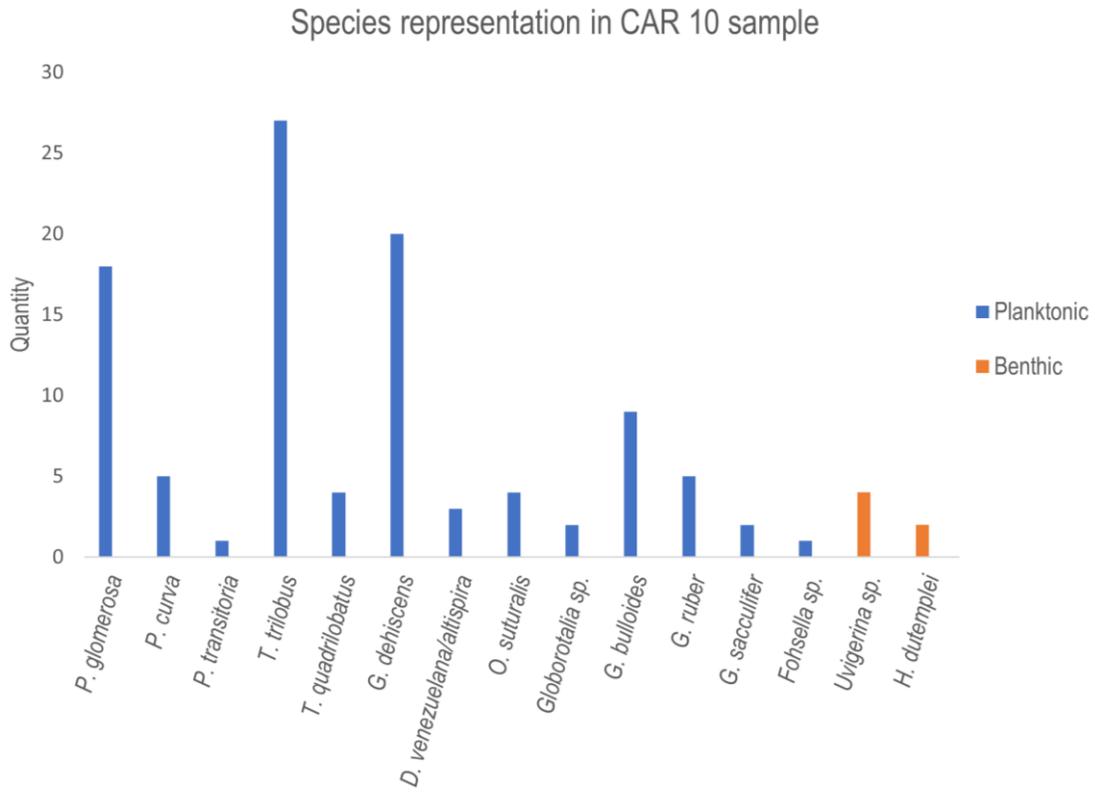
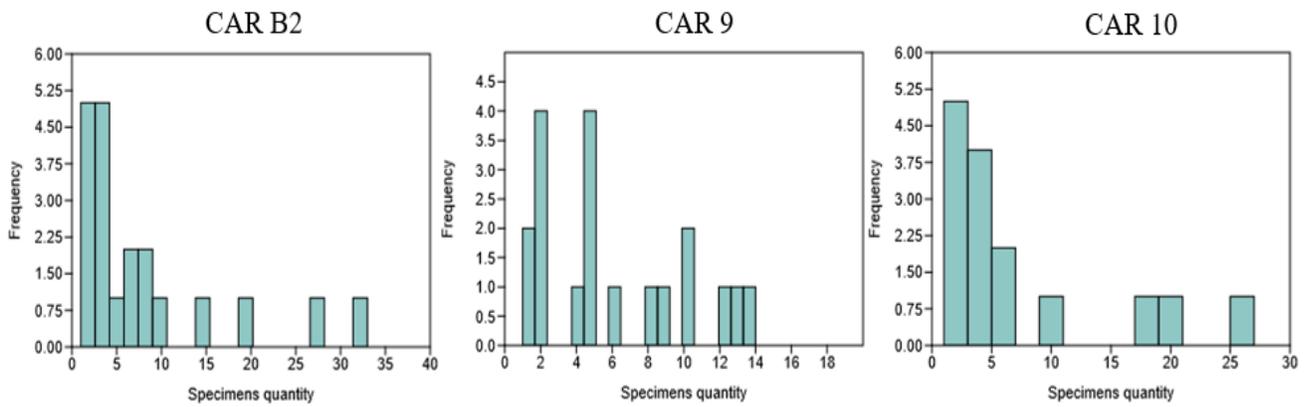


Figure 7. Identified foraminiferal species and their abundance in the CAR 10 sample.

Figure 8. Histograms of species distribution in the analyzed samples.



3.5. Discussion

The sample CAR B2 is represented only by planktonic foraminifera without a normal distribution of the taxa, see Fig. 6. The most abundant genus is the genus *Trilobatus* (*Globigerinoides*) (68 species, 42% of the total sample, see Table 3), mainly represented by *T. trilobus*, *T. immaturus*, *T. sacculifer* and the *T. quadrilobatus* species. Each of these species has a comparable ecology, in fact, *T. quadrilobatus*, *T. immaturus*, and *T. trilobus* can be considered as evolutionary morphotypes of *T. sacculifer* (André *et al.*, 2013). According to the literature, *T. trilobus* and *T. sacculifer* are surface dwellers, that are very abundant in the tropical to subtropical open ocean waters (Tolderlund & Bé, 1971; Pearson *et al.*, 1997; Aze *et al.*, 2011). Hemleben *et al.* (1989) reported a temperature tolerance of 14–31°C for *T. trilobus* and described *T. immaturus* and *T. quadrilobatus* as cosmopolitan species. Nikolaev *et al.* (1998) reported a surface habitat range for these two species between ~25 and 100 m. All four species of the genus *Trilobatus* mentioned are known to be rather oligotrophic environmental indicators (Schiebel & Hemleben, 2017). A similar habitat has been proposed for *Globigerinoides ruber* and *Dentoglobigerina*. *G. ruber* lives mainly in the upper 50 m of the water column (Peeters, 2002). It is a salinity-tolerant species that can be found in different ecological habitats (most commonly in subtropical to tropical habitats; Scott, 2020). Similar to *Trilobatus* genera, *G. ruber* prefers rather oligotrophic conditions (Toledo, 2008). It is a symbiont-bearing species like *T. sacculifer* and *O. universa* (Schiebel & Hemleben, 2017). Both, *Dentoglobigerina altispira* and *Dentoglobigerina venezuelana*, are also symbiont-bearing, surface-dwelling species with a preference for a tropical to subtropical climate (Aze *et al.*, 2011). Furthermore, the presence of *Orbulina* and *Praeorbulina* supports the presumed oligotrophic conditions, as these genera are also considered as oligotrophic markers, and *O. universa* is reported to be found at depths of up to 100 m (Bemis *et al.*, 2000; Lekieffre *et al.*, 2020). Both, *Orbulina* and *Praeorbulina* are reported as cosmopolitan genera with symbionts and they are known to tolerate a wide range of temperature and salinity fluctuations, thriving mainly in tropical and temperate waters (Drinia *et al.*, 2007; Schiebel & Hemleben, 2017). In total, there are 11 taxa that are indicative of warm and oligotrophic water conditions (comprising 117 specimens, 73% of the total assemblage). On the contrary, there are two taxa (18 specimens, 11%), that are indicative of rather nutrient-rich surface waters. These are *Globigerinella obesa* and *Globigerina bulloides*. *G. obesa* is mainly reported from tropical to temperate climates, and assemblages dominated by *G. obesa* represent high nutrient surface waters (Öğretmen, 2022; Di Stefano *et al.*, 2010). *G. bulloides* is a symbiont-barren species, which is characteristic for eutrophic (high nutrient) surface waters and it is tolerant to a wide range of temperatures (Schiebel & Hemleben, 2017; Öğretmen, 2022). Schiebel *et al.* (2017) associate *G. bulloides* with a preference for cooler waters (temperate to subpolar). Finally, the assemblage contains also *Globoquadrina dehiscens* (14 specimens), which is a cosmopolitan species with a variable life-strategy and is therefore not significant as

an environmental marker (Fabbrini & Foresi, 2020). Overall, the composition of the assemblage suggests that the environment of the CAR B2 sample reflects oligotrophic, warm water, open ocean conditions, but with periods of the water column instability (rainfall periods, freshwater and high nutrient inputs) based on the presence of *G. bulloides* and *G. obesa*.

In sample CAR 9, the data are normally distributed, according to the normality test, see Fig. 8. The planktonic species in the analyzed assemblage are predominantly represented by *T. trilobatus*, *T. quadrilobatus*, *T. sacculifer*, *G. ruber*, *D. venezuelana*, *D. altispira* species and the genera *Orbulina*, *Praeorbulina* (see Table 4), all of which represents warm water species that prefer tropical to subtropical climates (e.g., Schiebel & Hemleben, 2017; Aze *et al.*, 2011). There is also the presence of *Globorotalia mayeri* (5 specimens; 5.3% of the total plankton assemblage), a mixed-layer to upper thermocline dwelling species (Leckie *et al.*, 2018). In the assemblage it is accompanied also by *Turborotalita* sp. (a *quinqueloba* species), which inhabits the same environments as the *G. mayeri* (Simstich *et al.*, 2003). Bé, (1977) reported, that *T. quinqueloba* prefers rather cold unstratified waters, but can also occur in the tropics under favourable conditions. In the analyzed assemblage there are 18% of benthic specimens, which allowed to apply the EBFOI index (EBFOI = 85) to calculate the average dissolved oxygen levels at the seafloor. Based on the result of this calculation, the DO (dissolved oxygen) value of 5.14[ml/l] indicates highly oxic conditions at the seafloor (Kranner *et al.*, 2022). The presence of *Heterolepa dutemplei* (12 specimens, 57% of the total benthic assemblage) and the *Martinotiella communis* (5 specimens, 24% of the total benthic assemblage) supports the dissolved oxygen value (DO) value given by the EBFOI calculation (Kranner *et al.*, 2022). *H. dutemplei* is considered as an oxic epifaunal species, inhabiting the top 1 cm of the sediment and preferring outer shelf environments (depths >60 m; Kovacova *et al.*, 2009; Russo *et al.*, 2022). *M. communis* is considered as an infaunal oxic species (preferring DO values between 4.7ml/l and 5.7ml/l; Harloff & Mackensen, 1997; Goubert *et al.*, 2001) and it can be found up to the bathyal zone (depths >200 m; Hanagata, 2006). In contrast, *Uvigerina* sp. and *Bolivina* sp. (2 specimens each in the analyzed assemblage) are both considered to be bathyal species, indicating rather lower DO levels but high organic matter contents (e.g., De Mello E Sousa *et al.*, 2006; Murray, 2006; Goubert *et al.*, 2001; Pippèr & Reichenbacher, 2010). Therefore, based on the assemblage composition and the calculation of the EBFOI index, a warm oligotrophic environment between the outer shelf and the bathyal zone can be suggested. The EBFOI calculation also suggests a rather high oxic environment at the seafloor, supported by the abundance and dominance of *Heterolepa dutemplei* and *Martinotiella communis* in the benthic assemblage.

Sample CAR 10 is dominated by planktonic foraminifera, with benthic foraminifera comprising only 5.6% of the assemblage. The Shapiro-Wilk test shows that the data do not have a normal distribution (see Fig. 10). The most abundant species are the representatives of oligotrophic, warm water species

(e.g., *T. trilobatus*, *T. quadrilobatus*, *G. ruber*, *Praeorbulina glomerosa*, *P. curva* and *P. suturalis*; Schiebel & Hemleben, 2017; Bemis *et al.*, 2000; see Table 5), which account for 69 out of the total 101 planktonic specimens (68.3%). *Globigerina bulloides* is the only significantly represented planktonic species (9 specimens in the total assemblage), indicating rather eutrophic cooler waters (Öğretmen, 2022). From the benthics the presence of *Uvigerina* sp. (4 specimens), which is considered as a shallow to intermediate infaunal suboxic species, indicates rather eutrophic cold conditions at the seafloor (Székely *et al.*, 2017). In contrast, *Heterolepa* sp. (2 specimens), which is an epifaunal species, indicates rather oligotrophic and oxic bottom water conditions (Murray, 2006; Russo *et al.*, 2022). Overall, the assemblage composition suggests rather oligotrophic warm water environment with periods of the water column instability based on the presence of the species *G. bulloides*. The benthic assemblage consists of only two species with different ecological preferences, making it impossible to draw any conclusions.

4. Conclusions

In all analyzed samples there is a dominance of planktonic species. In sample CAR B2 the benthic assemblage is completely absent, in sample CAR 9 it represents 18%, while in sample CAR 10 it represents only 5.6%. The planktonic species in all three samples are dominated by oligotrophic indicators, such as representatives of the genus *Trilobatus* or *Praeorbulina/Orbulina*. The assemblages also contain markers of eutrophic, nutrient-rich surface waters such as *Globigerina bulloides* (all three samples), *Globigerinella obesa* (CAR B2), *Globorotalia mayeri* and *Turborotalita quinqueloba* (CAR 9). Overall, this suggests a primarily oligotrophic, warm-water, open-ocean environment with periods of water column instability (e.g. freshwater input). In the case of sample CAR 9, using the EBFOI calculation and the composition of the benthic assemblage with the dominance of *Heterolepa dutemplei* and *Martinotiella communis* suggests a rather highly oxic environment from the outer shelf to the bathyal zone.

5. References

Abrantes, F., Voelker, A. H., Sierro Sanchez, F. J., Naughton, F., Rodrigues, T., Cacho, I., ... & Batista, L. F. (2010). Paleoclimate variability in the Mediterranean region. *Mediterranean Climate: from Past to the Future*.

Ahmed, M. J., Tamar-Agha, M. Y., & Alwan, T. A. (2017). The Sedimentology and Facies Analysis of the Cretaceous Oceanic Red Beds (CORBs) in the Shiranish Formation, Northern of Iraq. *Iraqi Journal of Science*, 1220-1234.

Aksu, A. E., Ulug, A., Piper, D. J. W., Konuk, Y. T., & Turgut, S. (1992). Quaternary sedimentary history of Adana, Cilicia and Iskenderun basins: northeast Mediterranean Sea. *Marine Geology*, 104(1-4), 55-71.

Alexander, E. M., Jago, J. B., Rozanov, A. Y., & Zhuravlev, A. Y. (2001). *The Cambrian biostratigraphy of the Stansbury Basin, South Australia* (Doctoral dissertation, Russian Academy of Sciences).

Anbar, A. D., & Knoll, A. H. (2002). Proterozoic ocean chemistry and evolution: a bioinorganic bridge?. *Science*, 297(5584), 1137-1142.

André, A., Weiner, A., Quillévéré, F., Aurahs, R., Morard, R., Douady, C. J., ... & Kucera, M. (2013). The cryptic and the apparent reversed: lack of genetic differentiation within the morphologically diverse plexus of the planktonic foraminifer *Globigerinoides sacculifer*. *Paleobiology*, 39(1), 21-39.

Aze, T., Ezard, T. H., Purvis, A., Coxall, H. K., Stewart, D. R., Wade, B. S., & Pearson, P. N. (2011). A phylogeny of Cenozoic macroperforate planktonic foraminifera from fossil data. *Biological Reviews*, 86(4), 900-927.

Bábek, O., Faměra, M., Hladil, J., Kapusta, J., Weinerová, H., Šimíček, D., ... & Ďurišová, J. (2018). Origin of red pelagic carbonates as an interplay of global climate and local basin factors: Insight from the Lower Devonian of the Prague Basin, Czech Republic. *Sedimentary geology*, 364, 71-88.

Bábek, O., Vodrážková, S., Kumpan, T., Kalvoda, J., Holá, M., & Ackerman, L. (2021). Geochemical record of the subsurface redox gradient in marine red beds: A case study from the Devonian Prague Basin, Czechia. *Sedimentology*, 68(7), 3523-3548.

Bai, H., Kuang, H., Liu, Y., Peng, N., Chen, X., & Wang, Y. (2020). Marinoan-aged red beds at Shennongjia, South China: Evidence against global-scale glaciation during the Cryogenian. *Palaeogeography, Palaeoclimatology, Palaeoecology*, 559, 109967.

Bailey, H. W. (2020). A brief review of the Late Cretaceous “Oceanic Red Beds” of the North Sea offshore region. *Proceedings of the Geologists' Association*, 131(5), 425-431.

- Bé, A. W., Hemleben, C., Anderson, O. R., Spindler, M., Hacunda, J., & Tuntivate-Choy, S. (1977).** Laboratory and field observations of living planktonic foraminifera. *Micropaleontology*, 155-179.
- Bekker, A., Slack, J. F., Planavsky, N., Krapez, B., Hofmann, A., Konhauser, K. O., & Rouxel, O. J. (2010).** Iron formation: the sedimentary product of a complex interplay among mantle, tectonic, oceanic, and biospheric processes. *Economic Geology*, 105(3), 467-508.
- Bemis, B. E., Spero, H. J., Lea, D. W., & Bijma, J. (2000).** Temperature influence on the carbon isotopic composition of *Globigerina bulloides* and *Orbulina universa* (planktonic foraminifera). *Marine Micropaleontology*, 38(3-4), 213-228.
- Bernhard, J. M., Edgcomb, V. P., Visscher, P. T., McIntyre-Wressnig, A., Summons, R. E., Bouxsein, M.L., ... & Jeglinski, M. (2013).** Insights into foraminiferal influences on microfabrics of microbialites at Highborne Cay, Bahamas. *Proceedings of the National Academy of Sciences*, 110(24), 9830-9834.
- Bialik, O. M., Frank, M., Betzler, C., Zammit, R., & Waldmann, N. D. (2019).** Two-step closure of the Miocene Indian Ocean Gateway to the Mediterranean. *Scientific reports*, 9(1), 8842.
- Bijma, J., Faber, W. W., & Hemleben, C. (1990).** Temperature and salinity limits for growth and survival of some planktonic foraminifers in laboratory cultures. *Journal of foraminiferal research*, 20(2), 95-116.
- Boltovskoy, E., & Wright, R. C. (Eds.). (2013).** *Recent foraminifera*. Springer Science & Business Media.
- Bouchal, J. M., Güner, T. H., & Denk, T. (2018).** Middle Miocene climate of southwestern Anatolia from multiple botanical proxies. *Climate of the Past*, 14(10), 1427-1440.
- Brandano, M., Cornacchia, I., & Tomassetti, L. (2017).** Global versus regional influence on the carbonate factories of Oligo-Miocene carbonate platforms in the Mediterranean area. *Marine and Petroleum Geology*, 87, 188-202.
- Brett, C. E., McLaughlin, P. I., Histon, K., Schindler, E., & Ferretti, A. (2012).** Time-specific aspects of facies: state of the art, examples, and possible causes. *Palaeogeography, Palaeoclimatology, Palaeoecology*, 367, 6-18.
- Burton, R. (2002).** *Miocene to recent stratigraphy, structural architecture and tectonic evolution of the Adana Basin, Southern Turkey* (Doctoral dissertation, Memorial University of Newfoundland).
- Burton-Ferguson, R., Aksu, A. E., Calon, T. J., & Hall, J. (2005).** Seismic stratigraphy and structural evolution of the Adana Basin, eastern Mediterranean. *Marine Geology*, 221(1-4), 189-222.
- Capella, W., Flecker, R., Hernández-Molina, F. J., Simon, D., Meijer, P. T., Rogerson, M., ... & Krijgsman, W. (2019).** Mediterranean isolation preconditioning the Earth System for late Miocene climate cooling. *Scientific Reports*, 9(1), 3795.

- Card, C. J., & Montenari, M. (2023).** Comparative geochemistry of Early Carboniferous marine red beds (MRBs) and their significance for deep time paleoceanographic reconstructions. *Sedimentary Geology*, *444*, 106313.
- Caron, D. A., Faber, W. W., & Bé, A. W. (1987).** Effects of temperature and salinity on the growth and survival of the planktonic foraminifer *Globigerinoides sacculifer*. *Journal of the marine biological association of the United Kingdom*, *67*(2), 323-341.
- Chen, Y., Jiang, H., Lai, X., Yan, C., Richoz, S., Liu, X., & Wang, L. (2015).** Early Triassic conodonts of Jiarong, Nanpanjiang Basin, southern Guizhou Province, South China. *Journal of Asian Earth Sciences*, *105*, 104-121.
- Chen, Z. Q., Harper, D. A., Grasby, S., & Zhang, L. (2022).** Editorial preface to special issue: Extreme environments and biotic responses during the Neoproterozoic-Phanerozoic transition. *Global and Planetary Change*, *215*, 103894.
- Cléroux, C., Cortijo, E., Anand, P., Labeyrie, L., Bassinot, F., Caillon, N., & Duplessy, J. C. (2008).** Mg/Ca and Sr/Ca ratios in planktonic foraminifera: Proxies for upper water column temperature reconstruction. *Paleoceanography*, *23*(3).
- Cordie, D. R., Dornbos, S. Q., & Marengo, P. J. (2019a).** Increase in carbonate contribution from framework-building metazoans through early Cambrian reefs of the Western Basin and Range, USA. *Palaios*, *34*(3), 159-174.
- Cordie, D. R., Dornbos, S. Q., Marengo, P. J., Oji, T., & Gonchigdorj, S. (2019b).** Depauperate skeletonized reef-dwelling fauna of the early Cambrian: insights from archaeocyathan reef ecosystems of western Mongolia. *Palaeogeography, Palaeoclimatology, Palaeoecology*, *514*, 206-221.
- Cornacchia, I., Agostini, S., & Brandano, M. (2018).** Miocene oceanographic evolution based on the Sr and Nd isotope record of the Central Mediterranean. *Paleoceanography and Paleoclimatology*, *33*(1), 31-47.
- Cornacchia, I., Brandano, M., & Agostini, S. (2021).** Miocene paleoceanographic evolution of the Mediterranean area and carbonate production changes: A review. *Earth-Science Reviews*, *221*, 103785.
- Cornel, R. M., & Schwertmann, U. (1996).** The iron oxides. Structure, properties, reactions and uses. *VCH: Weinheim*.
- Crockford, P. W., Hayles, J. A., Bao, H., Planavsky, N. J., Bekker, A., Fralick, P. W., ... & Wing, B. A. (2018).** Triple oxygen isotope evidence for limited mid-Proterozoic primary productivity. *Nature*, *559*(7715), 613-616.
- Cumberpatch, Z. A., Soutter, E. L., Kane, I. A., Casson, M., & Vincent, S. J. (2021).** Evolution of a mixed siliciclastic-carbonate deep-marine system on an unstable margin: The Cretaceous of the Eastern Greater Caucasus, Azerbaijan. *Basin Research*, *33*(1), 612-647.

- Darbaş, G., & Nazik, A. (2010).** Micropaleontology and paleoecology of the Neogene sediments in the Adana Basin (South of Turkey). *Journal of Asian Earth Sciences*, 39(3), 136-147.
- DERMAN, A., & Gürbüz, K. (2007).** Nature, provenance and relationships of Early Miocene palaeovalley fills, northern Adana Basin, Turkey: their significance for sediment-bypassing on a carbonate shelf. *Turkish Journal of Earth Sciences*, 16(2), 181-209.
- Di Stefano, A., Verducci, M., Lirer, F., Ferraro, L., Iaccarino, S. M., Hüsing, S. K., & Hilgen, F. J. (2010).** Paleoenvironmental conditions preceding the Messinian Salinity Crisis in the Central Mediterranean: integrated data from the Upper Miocene Trave section (Italy). *Palaeogeography, Palaeoclimatology, Palaeoecology*, 297(1), 37-53.
- Drinia, H., Antonarakou, A., Tsaparas, N., & Kontakiotis, G. (2007).** Palaeoenvironmental conditions preceding the Messinian Salinity Crisis: A case study from Gavdos Island. *Geobios*, 40(3), 251-265.
- E Sousa, S. H. D. M., Passos, R. F., Fukumoto, M., da Silveira, I. C. A., Figueira, R. C. L., Koutsoukos, E. A., ... & Rezende, C. E. (2006).** Mid-lower bathyal benthic foraminifera of the Campos Basin, Southeastern Brazilian margin: Biotopes and controlling ecological factors. *Marine Micropaleontology*, 61(1-3), 40-57.
- Elorza, J., Gómez-Alday, J. J., & Berrocoso, Á. J. (2021).** Syndepositional processes in the pigmentation of oceanic red beds: evidence from the Basque–Cantabrian Basin (northern Spain). *Geological Magazine*, 158(9), 1683-1703.
- Evans, D., Brierley, C., Raymo, M. E., Erez, J., & Müller, W. (2016).** Planktic foraminifera shell chemistry response to seawater chemistry: Pliocene–Pleistocene seawater Mg/Ca, temperature and sea level change. *Earth and Planetary Science Letters*, 438, 139-148.
- Fairbanks, R. G., Sverdrlove, M., Free, R., Wiebe, P. H., & Bé, A. W. (1982).** Vertical distribution and isotopic fractionation of living planktonic foraminifera from the Panama Basin. *Nature*, 298(5877), 841-844.
- Fallaw, W. C. (1979).** A test of the Simpson coefficient and other binary coefficients of faunal similarity. *Journal of Paleontology*, 1029-1034.
- Faranda, C., Gliozzi, E., Cipollari, P., Grossi, F., Darbaş, G., Gürbüz, K., ... & Cosentino, D. (2013).** Messinian paleoenvironmental changes in the easternmost Mediterranean Basin: Adana Basin, southern Turkey. *Turkish Journal of Earth Sciences*, 22(5), 839-863.
- Feldmeijer, W., Metcalfe, B., Brummer, G. J., & Ganssen, G. M. (2015).** Reconstructing the depth of the permanent thermocline through the morphology and geochemistry of the deep dwelling planktonic foraminifer *Globorotalia truncatulinoides*. *Paleoceanography*, 30(1), 1-22.
- Flower, B. P., & Kennett, J. P. (1995).** Middle Miocene deepwater paleoceanography in the southwest Pacific: relations with East Antarctic Ice Sheet development. *Paleoceanography*, 10(6), 1095-1112.

- Foster, G. L., & Rae, J. W. (2016).** Reconstructing ocean pH with boron isotopes in foraminifera. *Annual Review of Earth and Planetary Sciences*, 44, 207-237.
- Franke, W., & Paul, J. (1980).** Pelagic redbeds in the Devonian of Germany—deposition and diagenesis. *Sedimentary Geology*, 25(3), 231-256.
- Gasson, E., DeConto, R. M., Pollard, D., & Levy, R. H. (2016).** Dynamic Antarctic ice sheet during the early to mid-Miocene. *Proceedings of the National Academy of Sciences*, 113(13), 3459-3464.
- Gill, B. C., Lyons, T. W., Young, S. A., Kump, L. R., Knoll, A. H., & Saltzman, M. R. (2011).** Geochemical evidence for widespread euxinia in the Later Cambrian ocean. *Nature*, 469(7328), 80-83.
- Giosan, L., Flood, R. D., & Aller, R. C. (2002).** Paleoceanographic significance of sediment color on western North Atlantic drifts: I. Origin of color. *Marine Geology*, 189(1-2), 25-41.
- González-Estrada, E., & Cosmes, W. (2019).** Shapiro–Wilk test for skew normal distributions based on data transformations. *Journal of Statistical Computation and Simulation*, 89(17), 3258-3272.
- Görür, N. (1979).** Downward development of overgrowths from echinoderm fragments in a submarine environment. *Sedimentology*, 26(4), 605-608.
- Görür, N. (1994).** Tectonic control in the development of a Lower-Middle Miocene reef at a complex triple junction: depositional history of the Karaisali Formation of the Adana Basin, Turkey. *Geologie Mediterranee*, 21(1), 49-67.
- Goubert, E., Néraudeau, D., Rouchy, J. M., & Lacour, D. (2001).** Foraminiferal record of environmental changes: Messinian of the Los Yesos area (Sorbas Basin, SE Spain). *Palaeogeography, Palaeoclimatology, Palaeoecology*, 175(1-4), 61-78.
- Gueguen, E., Doglioni, C., & Fernandez, M. (1998).** On the post-25 Ma geodynamic evolution of the western Mediterranean. *Tectonophysics*, 298(1-3), 259-269.
- Guitián, J., & Stoll, H. M. (2021).** Evolution of sea surface temperature in the southern mid-latitudes from late Oligocene through early Miocene. *Paleoceanography and Paleoclimatology*, 36(9), e2020PA004199.
- Gündem, C. Y. (2019).** Archaeozoological study of a unique Late Neolithic pit from Tepecik-Çiftlik, central Turkey. *Anthropozoologica*, 54(1), 97-110.
- Hallock, P., & Glenn, E. C. (1986).** Larger foraminifera: a tool for paleoenvironmental analysis of Cenozoic carbonate depositional facies. *Palaios*, 55-64.
- Hammer, Ø., & Harper, D. A. T. PD RYAN, 2001.** PAST: Paleontological Statistics Software Package for Education and Data Analysis. *Palaeontologia Electronica*, 4(1), 9.

- Hanagata, S.** (2006). Foraminiferal proxies of dissolved oxygen and their changes across the Miocene/Pliocene boundary in the Japan Sea. *Stratigraphy*, 3, 285-306.
- Harloff, J., & Mackensen, A.** (1997). Recent benthic foraminiferal associations and ecology of the Scotia Sea and Argentine Basin. *Marine Micropaleontology*, 31(1-2), 1-29.
- He, W., Yang, Z., Hu, J., Zhang, K., & Li, H.** (2023). Color Origin of Red Beds within the Danxia Basin, Southern China. *Minerals*, 13(8), 1054.
- Hemleben, C., Spindler, M., Anderson, O. R., Hemleben, C., Spindler, M., & Anderson, O. R.** (1989). Taxonomy and species features. *Modern planktonic foraminifera*, 8-32.
- Henderson, G. M.** (2002). New oceanic proxies for paleoclimate. *Earth and Planetary Science Letters*, 203(1), 1-13.
- Hodgskiss, M. S. W., & Sperling, E. A.** (2019a). Stratigraphy and shale geochemistry of the Belcher Group, Belcher Islands, southern Nunavut. *Summary of Activities*, 65-78.
- Hodgskiss, M. S., Crockford, P. W., Peng, Y., Wing, B. A., & Horner, T. J.** (2019b). A productivity collapse to end Earth's Great Oxidation. *Proceedings of the National Academy of Sciences*, 116(35), 17207-17212.
- Hönisch, B., & Hemming, N. G.** (2005). Surface ocean pH response to variations in pCO₂ through two full glacial cycles. *Earth and Planetary Science Letters*, 236(1-2), 305-314.
- Hu, X., Jansa, L., Wang, C., Sarti, M., Bak, K., Wagneich, M., ... & Sotak, J.** (2005). Upper Cretaceous oceanic red beds (CORBs) in the Tethys: occurrences, lithofacies, age, and environments. *Cretaceous Research*, 26(1), 3-20.
- Hu, X., Scott, R. W., Cai, Y., Wang, C., & Melinte-Dobrinescu, M. C.** (2012). Cretaceous oceanic red beds (CORBs): Different time scales and models of origin. *Earth-Science Reviews*, 115(4), 217-248.
- İlgar, A., Nemeç, W., Hakyemez, A., & Karakuş, E.** (2013). Messinian forced regressions in the Adana Basin: a near-coincidence of tectonic and eustatic forcing. *Turkish Journal of Earth Sciences*, 22(5), 864-889.
- Jenkyns, H. C.** (1988). The early Toarcian (Jurassic) anoxic event; stratigraphic, sedimentary and geochemical evidence. *American Journal of Science*, 288(2), 101-151.
- Jiang, S. Y., Pi, D. H., Heubeck, C., Frimmel, H., Liu, Y. P., Deng, H. L., ... & Yang, J. H.** (2009). Early Cambrian ocean anoxia in south China. *Nature*, 459(7248), E5-E6.
- Kaiho, K.** (1994). Benthic foraminiferal dissolved-oxygen index and dissolved-oxygen levels in the modern ocean. *Geology*, 22(8), 719-722.
- Karig, D. E., & Kozlu, H.** (1990). Late Palaeogene-Neogene evolution of the triple junction region near Maraş, south-central Turkey. *Journal of the Geological Society*, 147(6), 1023-1034.

- Kelling, G., Gökçen, S. L., Floyd, P. A., & Gökçen, N. (1987).** Neogene tectonics and plate convergence in the eastern Mediterranean: new data from southern Turkey. *Geology*, *15*(5), 425-429.
- Kiipli, E., Kallaste, T., & Kiipli, T. (2000).** Hematite and goethite in Telychian marine red beds of the East Baltic. *GFF*, *122*(3), 281-286.
- King, D. J., Wade, B. S., Liska, R. D., & Miller, C. G. (2020).** A review of the importance of the Caribbean region in Oligo-Miocene low latitude planktonic foraminiferal biostratigraphy and the implications for modern biogeochronological schemes. *Earth-science reviews*, *202*, 102968.
- Konhauser, K. O., Planavsky, N. J., Hardisty, D. S., Robbins, L. J., Warchola, T. J., Haugaard, R., ... & Johnson, C. M. (2017).** Iron formations: A global record of Neoarchaeon to Palaeoproterozoic environmental history. *Earth-Science Reviews*, *172*, 140-177.
- Kouchinsky, A., Alexander, R., Bengtson, S., Bower, F., Clausen, S., Holmer, L. E., ... & Zhuravlev, A. (2022).** Lower–Middle Cambrian faunas and stratigraphy from northern Siberia. *Acta Palaeontologica Polonica*, *67*, 341-464.
- Kováčová, P., Emmanuel, L., Hudáčková, N., & Renard, M. (2009).** Central Paratethys paleoenvironment during the Badenian (Middle Miocene): evidence from foraminifera and stable isotope ($\delta^{13}\text{C}$ and $\delta^{18}\text{O}$) study in the Vienna Basin (Slovakia). *International Journal of Earth Sciences*, *98*, 1109-1127.
- Kranner, M., Harzhauser, M., Beer, C., Auer, G., & Piller, W. E. (2022).** Calculating dissolved marine oxygen values based on an enhanced Benthic Foraminifera Oxygen Index. *Scientific reports*, *12*(1), 1376.
- Kučera, M. (2007).** Chapter six planktonic foraminifera as tracers of past oceanic environments. *Developments in marine geology*, *1*, 213-262.
- Leckie, R. M., Wade, B. S., Pearson, P. N., Fraass, A. J., King, D. J., Olsson, R. K., ... & Berggren, W. A. (2000).** Taxonomy, biostratigraphy, and phylogeny of Oligocene and early Miocene Paragloborotalia and Parasubbotina.
- Lekieffre, C., Spero, H. J., Fehrenbacher, J. S., Russell, A. D., Ren, H., Geslin, E., & Meibom, A. (2020).** Ammonium is the preferred source of nitrogen for planktonic foraminifer and their dinoflagellate symbionts. *Proceedings of the Royal Society B*, *287*(1929), 20200620.
- Lenton, T. M., & Daines, S. J. (2017).** Biogeochemical transformations in the history of the ocean. *Annual Review of Marine Science*, *9*, 31-58.
- Li, G., Jiang, G., & Wan, X. (2011).** The age of the Chuangde Formation in Kangmar, southern Tibet of China: Implications for the origin of Cretaceous oceanic red beds (CORBs) in the northern Tethyan Himalaya. *Sedimentary Geology*, *235*(1-2), 111-121.

- Li, G., Jiang, G., Hu, X., & Wan, X. (2009).** New biostratigraphic data from the Cretaceous Bolinxiala Formation in Zanda, southwestern Tibet of China, and their paleogeographic and paleoceanographic implications. *Cretaceous Research*, 30(4), 1005-1018.
- Li, M., Song, H., Wignall, P. B., She, Z., Dai, X., Song, H., & Xiao, Q. (2019).** Early Triassic oceanic red beds coupled with deep sea oxidation in South Tethys. *Sedimentary geology*, 391, 105519.
- Li, Y., Li, F., Kershaw, S., Burne, R., Wang, X., Lu, C., ... & Li, Y. (2023).** Extensive occurrences of lower Cambrian red beds in South China: Composition, characteristics, and implications for global environmental change. *Marine and Petroleum Geology*, 157, 106475.
- Luan, X. C., Wu, R. C., Zhan, R. B., & Liu, J. B. (2019).** The Zitai Formation in South China: unique deeper-water marine red beds in terms of lithology, distribution and $\delta^{13}\text{C}_{\text{carb}}$ chemostratigraphy. *Palaeoworld*, 28(1-2), 198-210.
- Lyu, X., Liu, Z., Wu, Q., Colin, C., Yu, X., Liu, C., & Li, Q. (2022).** Quantifying Iron oxide mineral contents in Miocene oceanic red beds for the deep-sea oxidation evolution in the South China Sea. *Frontiers in Earth Science*, 10.
- Mamet, B., & Pr eat, A. (2006).** Iron-bacterial mediation in Phanerozoic red limestones: state of the art. *Sedimentary Geology*, 185(3-4), 147-157.
- Meijer, P. T., Slingerland, R., & Wortel, M. J. R. (2004).** Tectonic control on past circulation of the Mediterranean Sea: a model study of the Late Miocene. *Paleoceanography*, 19(1).
- Melinte-Dobrinescu, M. C., Jipa, D., Brustur, T., & Szobotka, S. (2009).** Eastern Carpathian Cretaceous oceanic red beds: lithofacies, biostratigraphy and paleoenvironment. *Cretaceous Oceanic Red Beds: Stratigraphy, Composition, Origins and Paleoclimatic Significance* SEPM Special Publication, 91, 111-119.
- Michalzik, D. (1991).** Facies sequence of Triassic-Jurassic red beds in the Sierra Madre Oriental (NE Mexico) and its relation to the early opening of the Gulf of Mexico. *Sedimentary geology*, 71(3-4), 243-259.
- Miki, T. (1992).** Sedimentologic and palaeoclimatic classification of Cretaceous red beds in East Asia: a general view. *Journal of Southeast Asian Earth Sciences*, 7(2-3), 179-184.
- Mourik, A. A., Abels, H. A., Hilgen, F. J., Di Stefano, A., & Zachariasse, W. J. (2011).** Improved astronomical age constraints for the middle Miocene climate transition based on high-resolution stable isotope records from the central Mediterranean Maltese Islands. *Paleoceanography*, 26(1).
- Murray, J. W. (2006).** *Ecology and applications of benthic foraminifera*. Cambridge university press.
- Nazik, A. (2004).** Planktonic foraminiferal biostratigraphy of the Neogene sequence in the Adana Basin, Turkey, and its correlation with standard biozones. *Geological Magazine*, 141(3), 379-387.

Naziklmaz, A., & Gurbuzlmaz, K. (1992). Karaisali-Catalan-Egner yöresi (KB Adana) alt-orta Miyosen yasli denizalti yelpazelerinin planktonik foraminifer biyostratigrafisi. *Türkiye jeoloji bülteni*, 35(1), 67-80.

Neuhuber, S., Wagerich, M., Wendler, I., & Spötl, C. (2007). Turonian oceanic red beds in the Eastern Alps: Concepts for palaeoceanographic changes in the Mediterranean Tethys. *Palaeogeography, Palaeoclimatology, Palaeoecology*, 251(2), 222-238.

Neumann, P., & Wagerich, M. (2009). Cretaceous oceanic red beds from the Pindos Basin of Greece: long-term siliceous pelagic deposition punctuated by anoxia.

Ni, Y., Foster, G. L., Bailey, T., Elliott, T., Schmidt, D. N., Pearson, P., ... & Coath, C. (2007). A core top assessment of proxies for the ocean carbonate system in surface-dwelling foraminifers. *Paleoceanography*, 22(3).

Nikolaev, S. D., Oskina, N. S., Blyum, N. S., & Bubenshchikova, N. V. (1998). Neogene–Quaternary variations of the Pole–Equator temperature gradient of the surface oceanic waters in the North Atlantic and North Pacific. *Global and Planetary Change*, 18(3-4), 85-111.

Öğretmen, N. (2022). Quantitative analysis of Calabrian planktic foraminifer assemblages and paleoecology of the Eastern Mediterranean from the onshore epibathyal sedimentary archives (Mersin, Turkey). *Yerbilimleri*, 43(1), 18-36.

Pawlowski, J., Holzmann, M., Berney, C., Fahrni, J., Gooday, A. J., Cedhagen, T., ... & Bowser, S. S. (2003). The evolution of early Foraminifera. *Proceedings of the National Academy of Sciences*, 100(20), 11494-11498.

Pearson, P. N., Shackleton, N. J., & Hall, M. A. (1997). Stable isotopic evidence for the sympatric divergence of *Globigerinoides trilobus* and *Orbulina universa* (planktonic foraminifera). *Journal of the Geological Society*, 154(2), 295-302.

Peeters, F. J., Brummer, G. J. A., & Ganssen, G. (2002). The effect of upwelling on the distribution and stable isotope composition of *Globigerina bulloides* and *Globigerinoides ruber* (planktic foraminifera) in modern surface waters of the NW Arabian Sea. *Global and Planetary Change*, 34(3-4), 269-291.

Pippèrr, M., & Reichenbacher, B. (2010). Foraminifera from the borehole Altdorf (SE Germany): proxies for Ottnangian (early Miocene) palaeoenvironments of the Central Paratethys. *Palaeogeography, Palaeoclimatology, Palaeoecology*, 289(1-4), 62-80.

Preat, A., De Ridder, C., & Gillan, D. (2018). Bacterial origin of the red pigmentation of Phanerozoic carbonate rocks: an integrated study of geology-biology-chemistry (Ernest Van den Broeck medallist lecture 2017). *Geologica Belgica*.

Reinhard, C. T., Planavsky, N. J., Gill, B. C., Ozaki, K., Robbins, L. J., Lyons, T. W., ... & Konhauser, K. O. (2017). Evolution of the global phosphorus cycle. *Nature*, 541(7637), 386-389.

- Roca, E., Sans, M., Cabrera, L., & Marzo, M. (1999).** Oligocene to Middle Miocene evolution of the central Catalan margin (northwestern Mediterranean). *Tectonophysics*, 315(1-4), 209-229.
- Rogerson, M., Rohling, E. J., Bigg, G. R., & Ramirez, J. (2012).** Paleooceanography of the Atlantic-Mediterranean exchange: Overview and first quantitative assessment of climatic forcing. *Reviews of Geophysics*, 50(2).
- Rong, J., Wang, Y., & Zhang, X. (2012).** Tracking shallow marine red beds through geological time as exemplified by the lower Telychian (Silurian) in the Upper Yangtze Region, South China. *Science China Earth Sciences*, 55, 699-713.
- Rushton, A. W. A. (2011).** A revised correlation of the Cambrian rocks in the British Isles. Geological Society of London.
- Russo, B., Ferraro, L., Correggia, C., Alberico, I., Foresi, L. M., Vallefucio, M., & Lirer, F. (2022).** Deep-water paleoenvironmental changes based on early-middle Miocene benthic foraminifera from Malta Island (Central Mediterranean). *Palaeogeography, Palaeoclimatology, Palaeoecology*, 586, 110722.
- Rutishauser, S., Erasmi, S., Rosenbauer, R., & Buchbach, R. (2017).** SARchaeology—Detecting palaeochannels based on high resolution radar data and their impact of changes in the settlement pattern in Cilicia (Turkey). *Geosciences*, 7(4), 109.
- Sagawa, T., Yokoyama, Y., Ikehara, M., & Kuwae, M. (2012).** Shoaling of the western equatorial Pacific thermocline during the last glacial maximum inferred from multispecies temperature reconstruction of planktonic foraminifera. *Palaeogeography, Palaeoclimatology, Palaeoecology*, 346, 120-129.
- Saraswat, R. (2015).** Non-destructive foraminiferal paleoclimatic proxies: A brief insight. *Proceedings of the Indian National Science Academy*, 81(2), 381-395.
- Schiebel, R., & Hemleben, C. (2017).** *Planktic foraminifers in the modern ocean* (Vol. 358). Berlin: Springer.
- Scott, G. H. (2020).** Zooplankters in an oligotrophic ocean: contrasts in the niches of *Globigerinoides ruber* and *Trilobatus sacculifer* (Foraminifera: Globigerinida) in the South Pacific. *Ecoscience*, 27(4), 269-278.
- Serra-Kiel, J., Hottinger, L., Caus, E., Drobne, K., Ferrandez, C., Jauhri, A. K., ... & Zakrevskaya, E. (1998).** Larger foraminiferal biostratigraphy of the Tethyan Paleocene and Eocene. *Bulletin de la Société géologique de France*, 169(2), 281-299.
- Silva, D. B. D., Cronin, B., Celik, H., Goldberg, K., Kneller, B. C., & Gürbüz, K. (2020).** Evolution of two overlapping sand-rich clastic submarine fans in the Lower Miocene Adana Basin, southern Turkey: Contribution from a new palaeocurrent analysis. *Turkish Journal of Earth Sciences*, 29(5), 764-784.

- Simstich, J., Sarnthein, M., & Erlenkeuser, H. (2003).** Paired $\delta^{18}\text{O}$ signals of *Neogloboquadrina pachyderma* (s) and *Turborotalita quinqueloba* show thermal stratification structure in Nordic Seas. *Marine Micropaleontology*, *48*(1-2), 107-125.
- Skupien, P., Bubík, M., Švábenická, L., Mikuláš, R., Vašíček, Z., & Matýsek, D. (2009).** Cretaceous oceanic red beds in the outer Western Carpathians, Czech Republic.
- Song, H., Jiang, G., Poulton, S. W., Wignall, P. B., Tong, J., Song, H., ... & Wang, C. (2017).** The onset of widespread marine red beds and the evolution of ferruginous oceans. *Nature Communications*, *8*(1), 399.
- Steinthorsdottir, M., Coxall, H. K., De Boer, A. M., Huber, M., Barbolini, N., Bradshaw, C. D., ... & Strömberg, C. A. E. (2021).** The Miocene: The future of the past. *Paleoceanography and Paleoclimatology*, *36*(4), e2020PA004037.
- Steph, S., Regenberg, M., Tiedemann, R., Mulitza, S., & Nürnberg, D. (2009).** Stable isotopes of planktonic foraminifera from tropical Atlantic/Caribbean core-tops: Implications for reconstructing upper ocean stratification. *Marine Micropaleontology*, *71*(1-2), 1-19.
- Super, J. R., Thomas, E., Pagani, M., Huber, M., O'Brien, C., & Hull, P. M. (2018).** North Atlantic temperature and pCO₂ coupling in the early-middle Miocene. *Geology*, *46*(6), 519-522.
- Székely, S. F., Bindu-Haitonic, R., Filipescu, S., & Bercea, R. (2017).** Biostratigraphy and paleoenvironmental reconstruction of the marine lower Miocene Chechiş Formation in the Transylvanian Basin based on foraminiferal assemblages. *Carnets Geol.*, *17*(2), 11.
- Tang, D., Ma, J., Shi, X., Lechte, M., & Zhou, X. (2020).** The formation of marine red beds and iron cycling on the Mesoproterozoic North China Platform. *American Mineralogist*, *105*(9), 1412-1423.
- Thomas, E. (2008).** Descent into the Icehouse. *Geology*, *36*(2), 191-192.
- Tolderlund, D. S., & Bé, A. W. (1971).** Seasonal distribution of planktonic foraminifera in the western North Atlantic. *Micropaleontology*, 297-329.
- Toledo, F. A., Costa, K. B., Pivel, M. A., & Campos, E. J. (2008).** Tracing past circulation changes in the western South Atlantic based on planktonic foraminifera. *Revista Brasileira de Paleontologia*, *11*(3), 169-178.
- Turner, P. (1980).** *Continental red beds*. Elsevier.
- Tzanova, A., Herbert, T. D., & Peterson, L. (2015).** Cooling Mediterranean Sea surface temperatures during the Late Miocene provide a climate context for evolutionary transitions in Africa and Eurasia. *Earth and Planetary Science Letters*, *419*, 71-80.

- Uchman, A., & Demircan, H. (1999).** Trace fossils of Miocene deep-sea fan fringe deposits from the Cingöz Formation, southern Turkey. In *Annales Societatis Geologorum Poloniae* (Vol. 69, No. 3-4, pp.125-135).
- Unlugenc, U. C. (1993).** *Controls on Cenozoic sedimentation in the Adana Basin, southern Turkey* (Doctoral dissertation, Keele University).
- Van de Schootbrugge, B., Bachan, A., Suan, G., Richoz, S., & Payne, J. L. (2013).** Microbes, mud and methane: cause and consequence of recurrent Early Jurassic anoxia following the end-Triassic mass extinction. *Palaeontology*, 56(4), 685-709.
- Wagreich, M., & Krenmayr, H. G. (2005).** Upper Cretaceous oceanic red beds (CORB) in the Northern Calcareous Alps (Nierental Formation, Austria): slope topography and clastic input as primary controlling factors. *Cretaceous Research*, 26(1), 57-64.
- Wagreich, M., Hu, X., & Sageman, B. (2011).** Causes of oxic–anoxic changes in Cretaceous marine environments and their implications for Earth systems—an introduction. *Sedimentary Geology*, 235(1-2), 1-4.
- Wang, C., Hu, X., Huang, Y., Wagreich, M., Scott, R., & Hay, W. (2011).** Cretaceous oceanic red beds as possible consequence of oceanic anoxic events. *Sedimentary geology*, 235(1-2), 27-37.
- Wang, H., Li, C., Cheng, M., Zhang, Z., & Algeo, T. J. (2022).** Redbed formation in the redox-stratified mid-Proterozoic ocean. *Precambrian Research*, 379, 106815.
- Wang, X., Zhang, S., Wang, H., Bjerrum, C. J., Hammarlund, E. U., Haxen, E. R., ... & Canfield, D. E. (2017).** Oxygen, climate and the chemical evolution of a 1400 million year old tropical marine setting. *American Journal of Science*, 317(8), 861-900.
- Wendler, J., Wendler, I., & Kuss, J. (2009).** Early Turonian shallow marine red beds on the Levant carbonate platform (Jordan), Southern Tethys.
- Westerhold, T., Marwan, N., Drury, A. J., Liebrand, D., Agnini, C., Anagnostou, E., ... & Zachos, J. C. (2020).** An astronomically dated record of Earth's climate and its predictability over the last 66 million years. *Science*, 369(6509), 1383-1387.
- Widiatama, A. J., Fahrudin, A., & Santy, L. D. (2021, November).** Characteristics of polymetallic enrichment on oceanic red bed in Matano Formation, Baturubei, Central Sulawesi, Indonesia. In *IOP Conference Series: Earth and Environmental Science* (Vol. 882, No. 1, p. 012045). IOP Publishing.
- Wignall, P. B., & Twitchett, R. J. (1996).** Oceanic anoxia and the end Permian mass extinction. *Science*, 272(5265), 1155-1158.
- Williams, G. D., Ünlügenç, U. C., Kelling, G., & Demirkol, C. (1995).** Tectonic controls on stratigraphic evolution of the Adana Basin, Turkey. *Journal of the Geological Society*, 152(5), 873-882.

- Xi, C. H. E. N., Chengshan, W. A. N. G., Xiumian, H. U., Yongjian, H. U. A. N. G., Pingkang, W., Jansa, L., & Xuan, Z. (2007).** Cretaceous oceanic red beds: distribution, lithostratigraphy and paleoenvironments. *Acta Geologica Sinica-English Edition*, 81(6), 1070-1086.
- Yetiş, C. (1988).** Reorganization of the Tertiary stratigraphy in the Adana Basin, southern Turkey. *Newsletters on Stratigraphy*, 20(1), 43-58.
- Yetiş, C., Kelling, G., Gökçen, S. L., & Baroz, F. (1995).** A revised stratigraphic framework for Later Cenozoic sequences in the northeastern Mediterranean region. *Geologische Rundschau*, 84, 794-812.
- You, Y., Huber, M., Müller, R. D., Poulsen, C. J., & Ribbe, J. (2009).** Simulation of the middle Miocene climate optimum. *Geophysical Research Letters*, 36(4).
- Yuan, L., Wang, Y., Cai, R., Jiang, Q., Wang, J., Li, B., ... & Zhou, G. (2012).** The origin of hematite nanowire growth during the thermal oxidation of iron. *Materials Science and Engineering: B*, 177(3), 327-336.
- Zachos, J. C., Dickens, G. R., & Zeebe, R. E. (2008).** An early Cenozoic perspective on greenhouse warming and carbon-cycle dynamics. *nature*, 451(7176), 279-283.
- Zachos, J., Pagani, M., Sloan, L., Thomas, E., & Billups, K. (2001).** Trends, rhythms, and aberrations in global climate 65 Ma to present. *science*, 292(5517), 686-693.
- Zhang, X. L., Wang, Y., Rong, J. Y., & Li, R. Y. (2014).** Pigmentation of the Early Silurian shallow marine red beds in South China as exemplified by the Rongxi Formation of Xiushan, southeastern Chongqing, central China. *Palaeoworld*, 23(3-4), 240-251.
- Ziegler, A. M., & McKerrow, W. S. (1975).** Silurian marine red beds. *American Journal of Science*, 275(1), 31-56.
- Zou, Y., Liu, D., Zhao, F., Kuang, H., Song, C., Sun, Y., ... & Cheng, J. (2020).** Reconstruction of nearshore chemical conditions in the Mesoproterozoic: evidence from red and grey beds of the Yangzhuang formation, North China Craton. *International Geology Review*, 62(11), 1433-1449.

6. WWW Resources

<https://stratigraphy.org>
<https://www.biorender.com>
<https://www.mikrotax.org>
<https://www.marinespecies.org>